DESIGN AND DEVOLPMENT OF AN MONODISPERSE AEROSOL GENERATOR

Dietmar van Eijsden
TU Delft

Summary

A study has been carried out at the Department of Chemical Engineering, Loughborough University of Technology (UK), to design and characterise a condensation type monodisperse aerosol generator. The design of this new generator was based on an already existing design, the MAGE (Monodisperse Aerosol GEnerator). The new generator has been shown to be very good at generating aerosol of 1-4 μm diameter.

A system to change the particle diameter using a condensation nuclei filter was developed and tested. Filtering the condensation nuclei is a very good method of increasing the size of aerosol particle produced. Measurements employing the nuclei filtration system showed a 100% efficiency of the fliter and the expected theoretical linear correlation between cube root of the particle diameter and condensation nuclei concentration.

The effect of a reheater on the aerosol size distribution was also studied. It was found that using heating tape as a reheater can improve aerosol monodispersity. This heating tape is used to maintain a high temperature in the tube carrying the seed aerosol and stearic acid vapour from the furnace to the first couple of centimetres of the condenser tube.

Vapour liquid bubbler efficiencies at various gas flow rates and temperatures were also calculated. Measurements and computer simulation of the preheater showed that the preheater doesn't heat the incoming nitrogen to the furnace temperature before it reaches the bubbler. It is therefore important to measure, and subsequently control, the temperature in the bubbler instead of in the furnace. Different gas flow and liquid heights in the bubbler will then not affect the size of aerosol produced at a given temperature.

Table of Contents

1 Introduction

A study has been undertaken as part of the graduation requirements of the undergraduate course in Chemical Engineering of the Technical University of Delft (The Netherlands). The practical work was done at Loughborough University of Technology (UK) at the Department of Chemical Engineering under supervision of Dr. J.I.T. Stenhouse and Ir. D. Walsh. The total project is supervised by Prof. Dr. B. Scarlett from Technical University of Delft.

The main goal of the of the study was to design and develop a condensation-type aerosol generator, based on the design of the Prodi aerosol generator (MAGE) [36], that would be an improvement on the original design, and to get more insight into the mechanisms of the processes involved in the aerosol generator, in order to generate monodisperse and predictable aerosols. The rig is called the IMAGE, Improved Monodisperse Aerosol GEnerator. It was hoped that when all mechanisms involved were sufficienctly well understood a mathematical model of the process could be developed.

Previous measurements with the MAGE at Loughborough had shown that disconnection of the reheater had no effect on the monodispersity of the aerosol produced, the effect of a reheater on product monodispersity was thus considered essential. Horton [1] reported that smaller particles were produced when there was a higher liquid level in the bubbler, so it was of interest to measure the effect of liquid height on particle size (the effect on mass-transfer). It was also intended to test a rapid method of increasing the size of aerosol produced by the generator, by using a filter that would remove the condensation nuclei.

The following objectives were dependant on the results of the results of the previous measurements.

This report has the following structure; chapter 2 reviews monodisperse aerosol technology, highlighting aerosol generation and methods to describe aerosol characteristics; chapter 3 describes the test rig and the aerosol characterisation equipment used; chapter 4 presents and discusses the results of the measurements made; while chapter 6 presents the conclusions made drawn from this work.

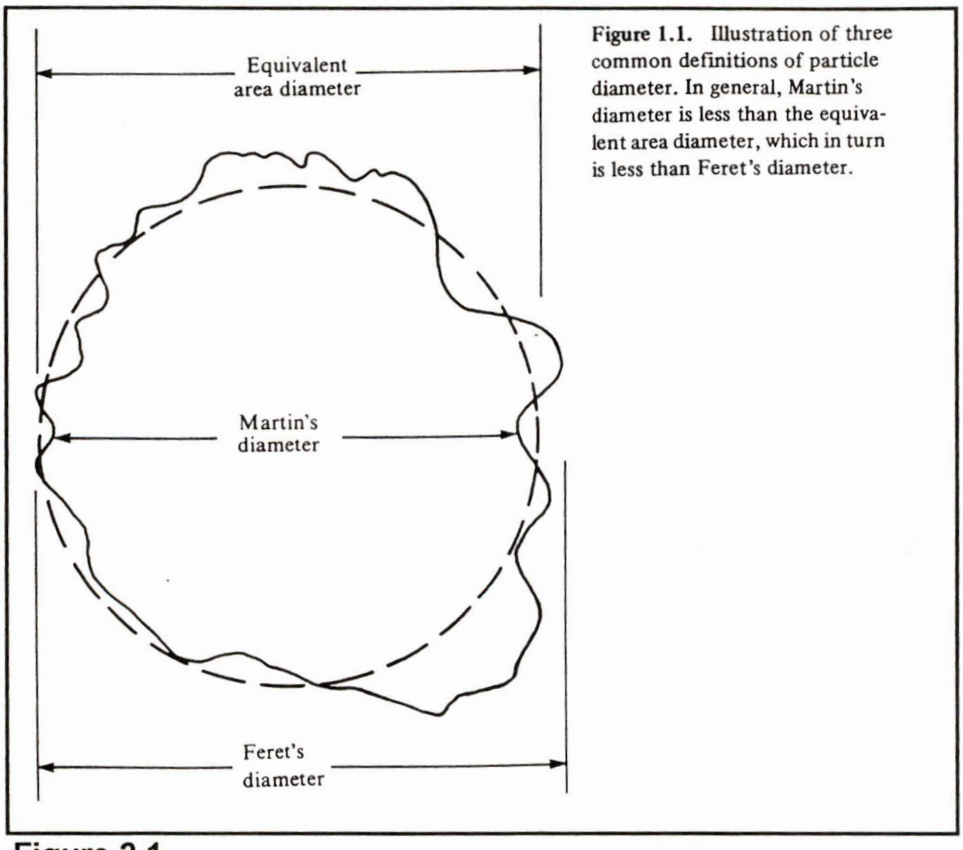

Figure 1.1. Illustration of three common definitions of particle diameter. In general, Martin's diameter is less than the equivalent area diameter, which in turn is less than Feret's diameter.

Figure 2.1

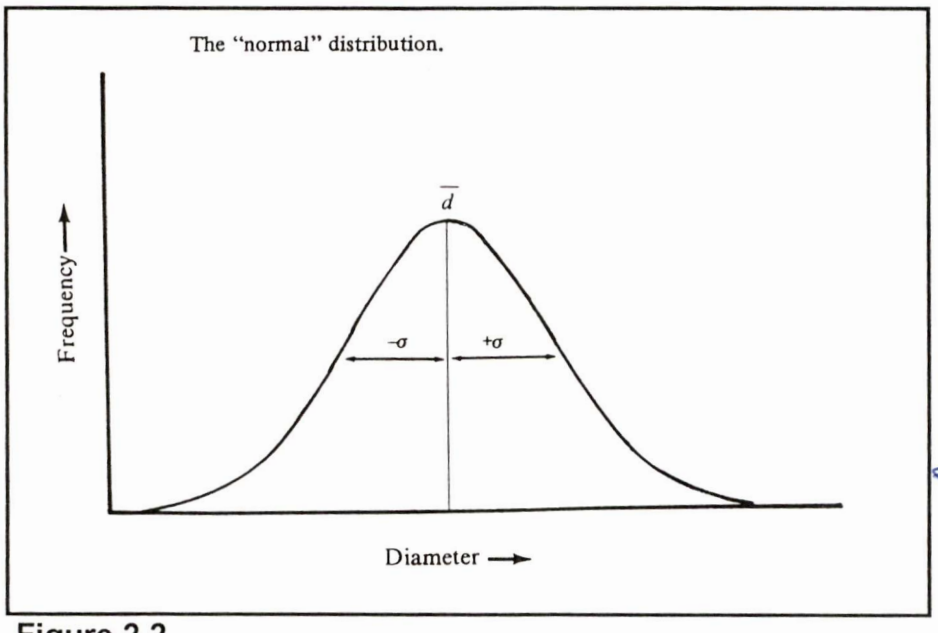

↑ volgende pag.

Figure 2.2

2 Review of Monodisperse Aerosol Technology

2.1 Introduction

An aerosol defined by The New Encyclopedia Britannica [2], ~~as~~ is a system of liquid or solid particles uniformly distributed in a divided state through a gas, usually air.

Typical properties by which aerosols are described are shape, number concentration, size, and size distribution [3].

Shape

It is convenient to think of all aerosols particles as spheres for calculation. But with the exception of fluid droplets, which are almost always spherical, many shapes are possible. These shapes can be devided into three general classes.

1. Isometric particles are those for which all three dimensions, in a carthesian co-ordinate system, are roughly the same. Spherical, regular polyhedral, or particles approximating these shapes belong in this class.

2. Plates are particles that have two long dimensions and a third small dimension. Leaves or leaf fragments, scales, and disks fall into this class.

3. Fibres are particles with a great length in one dimension compared to the other two. Examples are prisms, needles, and threads or mineral fibres such as asbestos.

Size

A particle is generally imagined to be spherical or nearly spherical. The two commonly encountered definition of particle size are Feret's diameter and Martin's diameter. These refer to estimates of approximate particle size when determined from viewing the projected images of a number of irregularly shaped particles. Feret's diameter is the maximum distance from edge to edge (figure 2.1) of each particle, and Martin's diameter is the length of each line that separates each particle into two equal portions. Since these measurements could vary depending on the orientation of the particle, they could only be valid if averaged over a large number of particles.

This measurement problem can be simplified somewhat by using the projected area diameter instead of Feret's or Martin's diameter. This is the defined as the area of a circle having the same projected area as the particle in question (shown in figure 2.1). In general Feret's diameter will be the larger than the projected area diameter which will be larger than Martin's diameter.

Sometimes a diameter is defined in terms of the particle settling velocity. All particles having similar settling velocities are considered to be of the same size, regardless of their actual size composition, or shape. Two such definitions which are most common are:

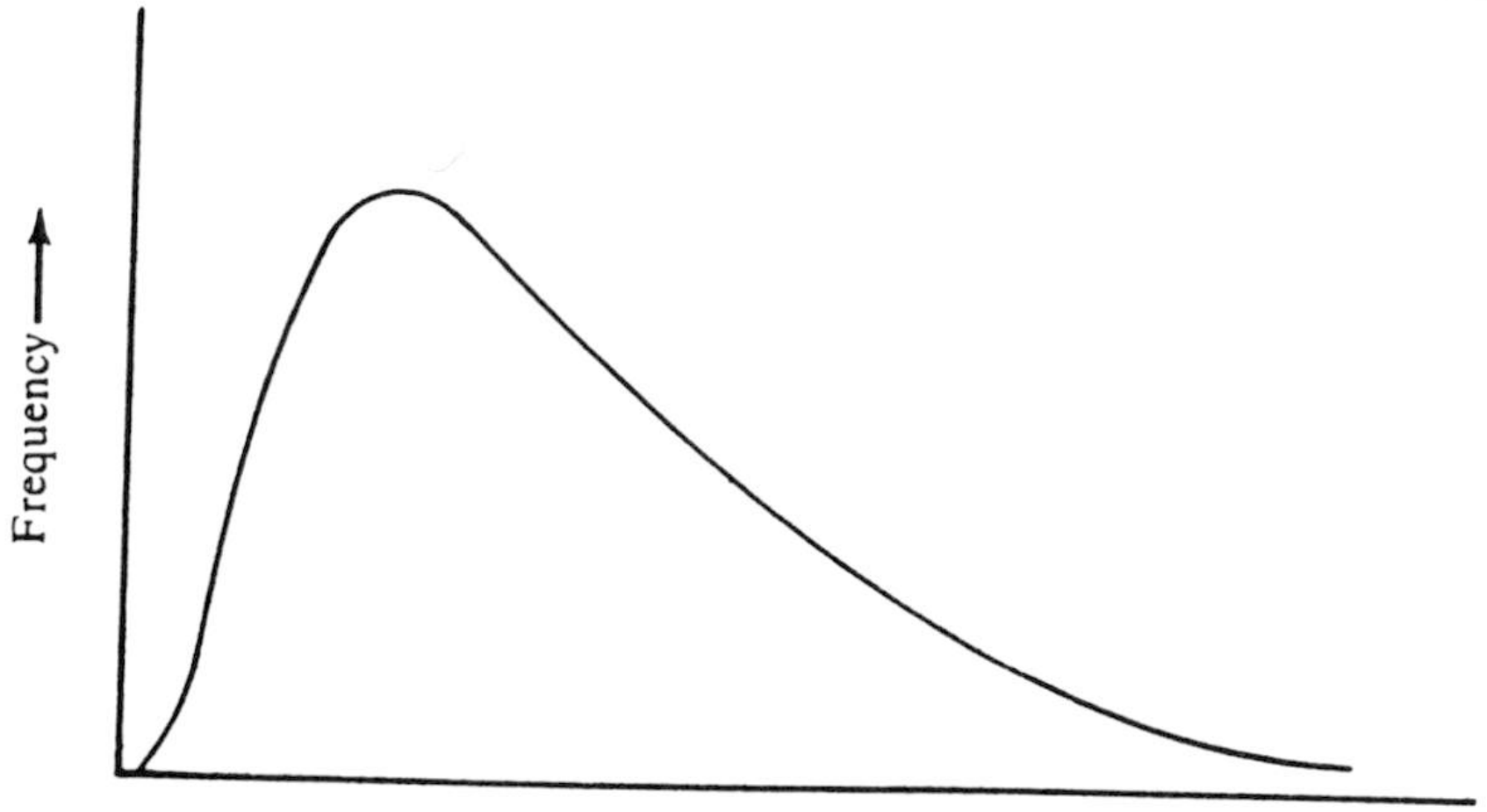

The "log-normal" distribution.

Figure 2.3

1. **Aerodynamic diameter** Diameter of a unit density sphere (density = 1 g/cm^3) having the same aerodynamic properties as the particle in question. This means that particles of the any shape or density will have the same aerodynamic diameter if their settling velocity is the same.

2. **Stokes diameter** Diameter of a sphere of the same density as the particle in question having the same settling velocity as that particle. Stokes diameter and aerodynamic diameter differ only in that the Stokes diameter includes the particle density whereas the aerodynamic diameter does not.

Particle Size Distribution

The number of particles in various size intervals can be plotted as bar charts or line charts. These plots are pictures of size distributions of the aerosol. This is useful in envisioning the range and frequency of the sizes present. If the size interval of the aerosol is permitted to become very small, the resultant histogram begins to approximate a smooth curve. It is then possible to represent the size distribution by a mathematical function. The classical mathematical curve is the normal distribution:

$$n(d) = \frac{1}{\sigma\sqrt{\pi}} \exp\left[-\frac{1}{2}\left(\frac{d-\bar{d}}{\sigma} \right)^2 \right] \qquad (2.1)$$

where

the mean diameter is defined by: $\bar{d} = \dfrac{\sum_{i=0}^{\infty} n_i d_i}{\sum_{i=0}^{\infty} n_i}$, (2.2)

the standard deviation by: $\sigma = \left[\dfrac{\sum_{i=0}^{\infty} n_i (\bar{d} - d_i)^2}{\sum_{i=0}^{\infty} n_i - 1} \right]^{1/2}$ (2.3)

and n the number of diameter d (m).

Means and standard deviations can be calculated for any set of data. For data which are normally distributed, however, the mean value lies at the midpoint of the data, and 67% of the distribution falls between the range of plus minus one standard deviation (as shown in figure 2.2). However many size distributions do not fit a normal distribution, but do fit a log normal distribution (shown in figure 2.3):

$$n(d) = \frac{1}{\log\sigma_g \sqrt{\pi}} \exp\left[-\frac{1}{2}\left(\frac{\log d - \log d_g}{\log \sigma_g} \right)^2 \right] \qquad (2.4)$$

where

the logarithmic mean diameter is defined by: $\log \bar{d}_g = \dfrac{\sum_{i=0}^{\infty} n_i \log d_i}{\sum_{i=0}^{\infty} n_i}$, (2.5)

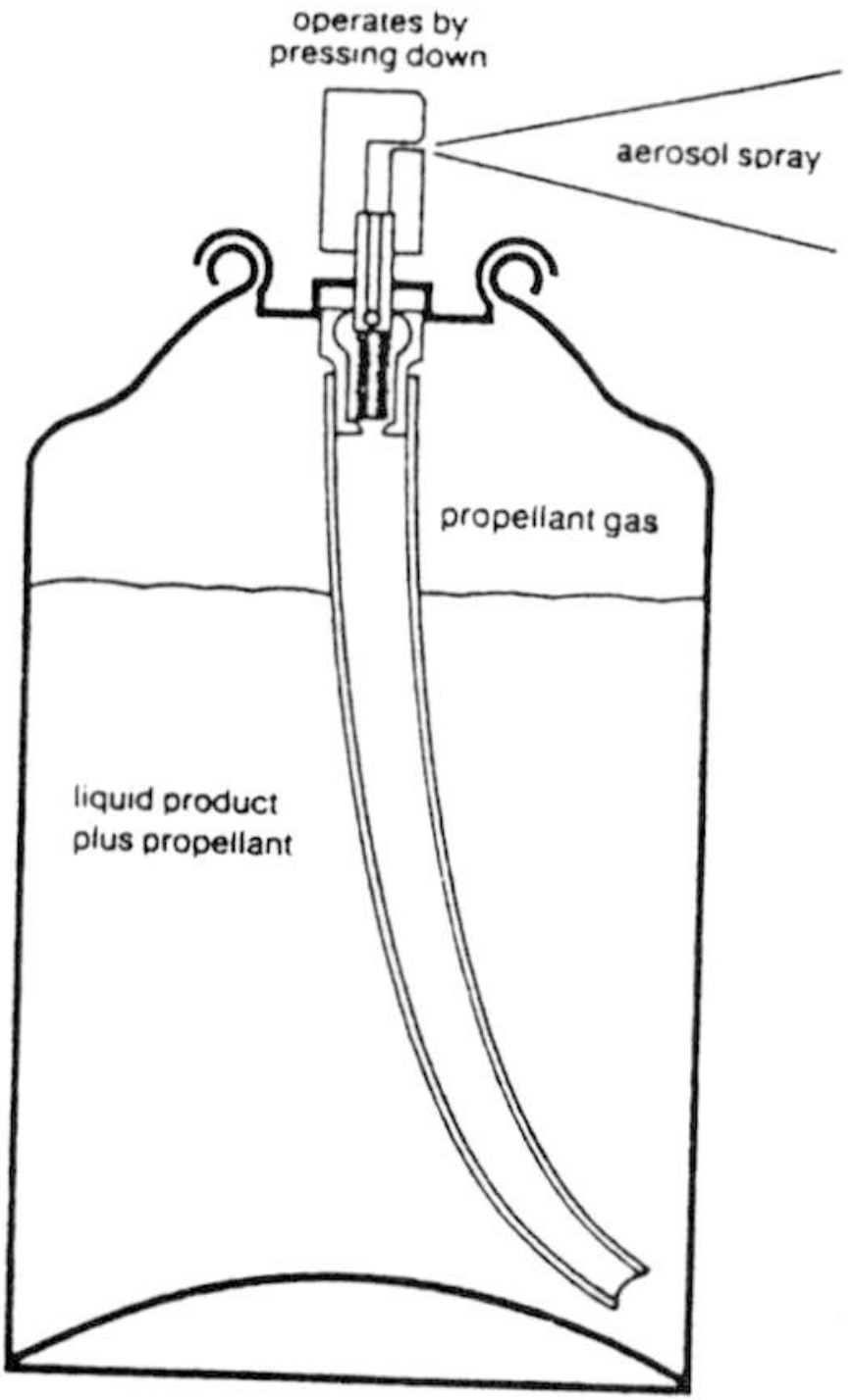

Cross section of a typical spray aerosol container

Figure 2.4

the geometric standard deviation by: $\log \sigma_g = \left[\frac{\sum_{i=0}^{\infty} n_i (\log \bar{d}_g - \log d_i)^2}{\sum_{i=0}^{\infty} n_i - 1} \right]^{1/2}$ (2.6)

and n the number of diameter d (m).

Monodispersity

The definition of monodispersity is central to the generation of aerosols. The most accepted definition, which was first presented by Fuchs and Sutugin [4], is that the coefficient of variation of the particle size distribution be less than 0.2. The coefficient of variation is described as the ratio of the standard deviation to the size distribution to the mean. For a log-normal distribution, the logarithm of the geometric standard deviation (GSD) must be less than 0.2 making the GSD less than 1.25. This criterion of practical monodispersity is, however, dependant on the accuracy of the method of the particle size analysis.

2.2 Requirements for Monodisperse Aerosols

When we think about aerosols in normal life, we think about pressurised cans (shown in figure 2.4), used for personal care (such as deodorant and hairspray), in the household (for cleaning purpose, insects sprays) and automotive products. [5]. These aerosols, however, do not require a high degree of monodispersity. Industrial and research activities require monodisperse aerosols. In the following section the use of monodisperse aerosols in research is summarised.

Monodisperse aerosols were made use of in the study of optical properties of aerosols, particle vibrations in the sonic field, inertial aerosol deposition on different bodies, aerosol deposition on pipe walls from a turbulent flow, deposition in impactors, in thermal and electrical precipitators, atomisation of bacterial suspension, methods of aerosol sampling, diffusion deposition from the flow in narrow channels, sedimentation and diffusion in a cell, aerosol filtration fibrous and granular filters, efficiency of droplet collisions with solid walls, particle charges in condensation aerosols acquired during their formation and by capture of gas ions, aerosol washing out by rain, relationship between insecticides and herbicides and the droplet size, supercooling of droplets and their vapour pressure, motion of coarse powders in pipes, lubrication of bearings with oil mists. Furthermore for the verification of the laws of Stokes and of Kelvin, for the calibration of instruments used for particle size determination in aerosols, photometers, electrostatic and centrifugal classifiers.

Industry has developed special techniques for the preparation of inorganic, organic, simple, composite, or coated powders [6]. Ceramic powders are used in the manufacture of pigments, substrates for catalysts and integrated circuits, silicone rubbers, highly tough ceramics, and superconductors [7]

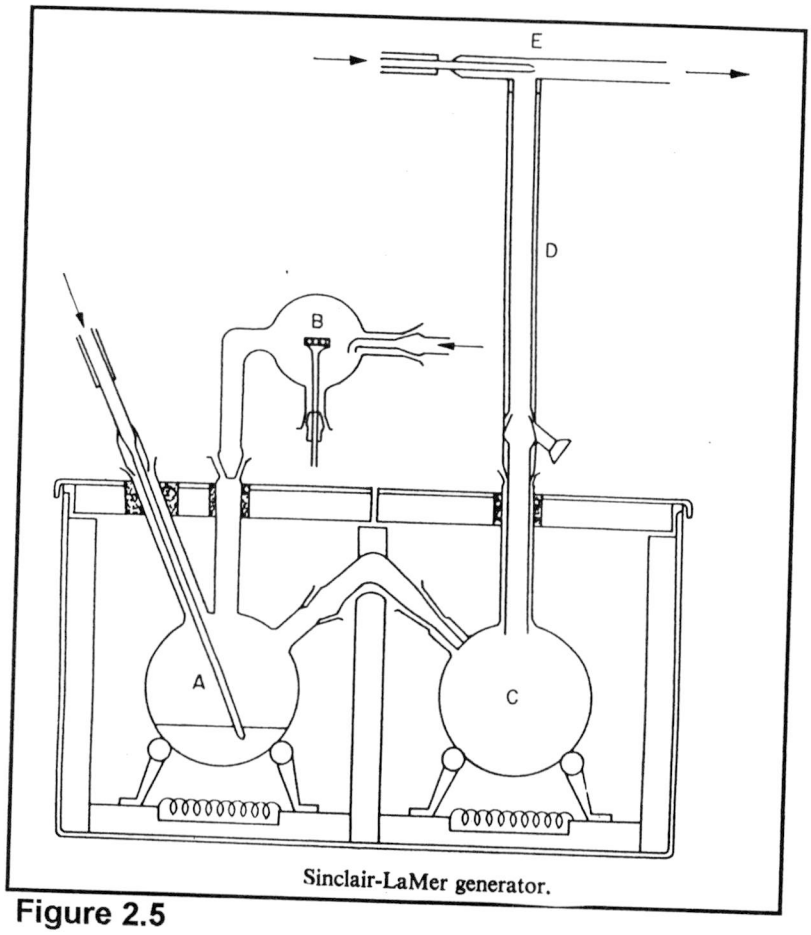

Sinclair-LaMer generator.

Figure 2.5

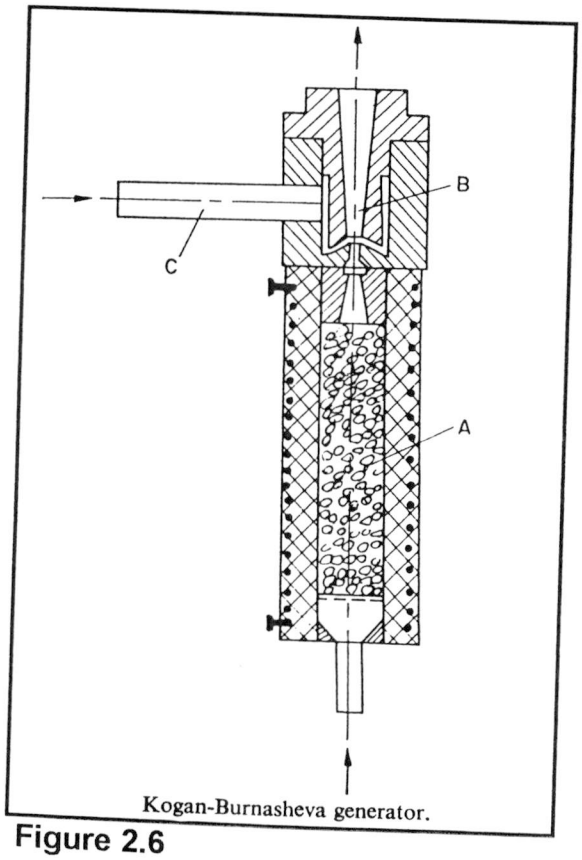

Kogan-Burnasheva generator.

Figure 2.6

2.3 Methods of Generation of Monodisperse Aerosols

2.3.1 Introduction

The two most applied methods of generating monodisperse aerosols are by condensation generation and by dispersing monodispersed particles. In this section the principles and examples of both methods are described.

2.3.2 Generation of Monodisperse Aerosols by Condensation Methods

2.3.2.1 Generation by Adiabatic Expansion of Vapour-Gas Mixtures

Rapid expanding of a vapour-gas mixture causes adiabatic cooling of the mixture. This cooling causes a super-saturation of the gas-phase, which starts to condense, and the grow of particles. Adiabatic expansion of moist atmospheric air containing a large number of condensation nuclei of greatly differing activity results in the formation of a very polydisperse mist. If this mist is allowed to disappear, partly by settling of the droplets and partly by evaporation, the largest and most active nuclei will be removed and the total number of nuclei will decrease considerably. A repeated expansion will produce a coarser and, as explained above, more monodisperse mists [8]. Only mists of volatile liquids (mainly of water) have so far been produced in this way and the estimation of the degree of monodispersity of these mists by direct measurements of the droplets is very difficult.

2.3.2.2 Aerosol Generators of the Heat-Exchanger Type

In a heat-exchanger type aerosol generator a highly boiling substance is evaporated into a carrier gas containing condensation nuclei. In a following section the gas-flow is reheated, causing a homogeneous gas mixture containing the nuclei. In the last section, the cooler, all of the highly boiling substance is condensed onto the nuclei to form monodisperse aerosol. Sinclair and LaMer [9-12] were the first to achieve generation aerosols by this way. The generator designed by them (figure 2.5) in 1941 was later widely used in aerosol investigation.

2.3.2.3 Aerosol Generators of the Mixer Type

The working principle of this type of aerosol generation is the mixing of a cold gas containing condensation nuclei and a gas-mixture containing the condensation gas, which causes the condensation onto the nuclei. This mixer type generator was designed by Kogan and Burnasheva [13]. The generator is shown in figure 2.6. Filtered gas is passed through a thermostat vaporiser (A) packed with granules of silica-gel impregnated with the liquid being vaporised. The cold gas containing the condensation nuclei enters through tube C and is mixed in nozzle B

2.3.3 Formation of Aerosols as a Result of a Chemical Process

The mechanism of this process is a gas phase reaction in which the reaction products are condensed to form the aerosols. Examples of this process is the condensation of methacrylate or methylmethacrylate under illumination of ultra-violet rays [14], and the mixing of air with water vapour and gas ions with NH_3 and HCl, to

form mists of aqueous solution of ammonium chloride were obtained [15].

2.3.4 Generation of Monodisperse Aerosols by Dispersion Methods

2.3.4.1 Generation by Atomisation of Liquids

The mechanism of atomisation of liquids is as follows: under the action of hydraulic pressure, a centrifugal or an aerodynamic force, the liquid is drawn into narrow ligaments or films [16], which subsequently disintegrate into droplets under the action of surface tension. The thinner the liquid ligament the smaller are droplets formed, but the degree of dispersity always remains large. On the other hand, when the liquid flows slowly out of a capillary tip, drops of a very constant size are formed, accompanied, however, by very small droplet satellites. Mechanical atomisation of liquids in atomisers, nozzles, etc. which is made use of in many fields of industry, gives as rule very polydisperse mists.

2.3.4.2 Generation by Atomisation of Suspensions

The atomisation of non-aggregated monodisperse suspension in water or some other volatile solvent, under such conditions that each droplet contains not more than one particle and the subsequent drying of the mist formed, should lead to monodisperse aerosols. There are two major problems in generation aerosols by this method. The first one is to get one particle in one droplet. The probability of presence of more than one particle in a droplet depends on the concentration of the suspension and on the relative size of particles and droplets. Let us assume the presence of 5% of twins in the aerosol to be admissible. Then according to Poisson's formula, with the mean droplet radius ~1 μm and with particle radius of 0.5, 0.25. 0.1, the concentrations should not exceed 1, 0,1, 0,01% respectively. The biggest difficulty is the presence of emulsifier in the suspension, which, cannot be completely eliminated. When the droplets containing no particles evaporate, "empty shells" remain. These empty shells can disturb the monodispersity. Examples of suspension from which aerosols are generated; lattices [17], bacteriophage T.3.E. Coli [18], and AgI [19].

2.3.4.3 Generation by Dispersion of Powders

The mechanism of this type of aerosol generation is quite simple. The dispersion of particles is caused by compressed air. Powders with a radius bigger than 10 μm are quite readily dispersed, but with decreasing particle size dispersion becomes increasingly difficult and for powders with radius smaller than 0.5 μm complete dispersion has not yet been achieved. In addition to the particle size, shape is of great importance and the elastic properties and humidity are also concerned. Plate and needle shaped particles are less readily dispersed than spherical ones; powders from hard substances are more readily dispersed than those of soft-ones; The presence of moisture in powders impairs their dispersion considerably, but if the powders are too dry, they also disperse less readily due to high triboelectric charges.

2.4 Measuring Techniques to Describe Aerosol Dimensions

2.4 Measuring Techniques to Describe Aerosol Dimensions

2.4.1 Microscopic Size Analysis

Microscope examination of a sample of dust collected on a slide is often the first step in determination of size and size distribution. This simple step yield valuable information on the size, whether the distribution is narrow or wide, and on the type of particulate. To obtain accurate information on the size distribution it is necessary to measure and size a large number of particles, in the order of 600, so the job is tedious and time consuming. A number of semi automatic and automatic systems have been introduced to increase the accuracy and ease of microscopic analysis. In the image shearing technique a double image of the particles is produced, coloured red and green by means of the filter, using a system of mirrors located belong the microscope eyepiece. The amount of shear and hence distance apart of the images is manipulated until the images just touch. The image shearing diameter of the particle is then read from the instrument . Particle counting aids are available.

Computer image analysis provides rapid and ambiased results. Care should be taken in interpreting results of automatic images analysis especially where edge effects may be important or where particles with concave surfaces are concerned.

The lower limit of particle size which can be measured using optical microscopy is about 1 μm using the oil immersion technique. Since the wavelength of light is about 0.5 μm adequate resolution of smaller particles is not feasible. In this case electron microscopy must be applied. Here because of the very short wavelength used, a very high resolution, in the order of 10 Å can be obtained. Since microscope slides are opaque to the electron beam a thin film which is transparent is used. The film which is about 100 Å thick is very fragile and is supported on a small grid about 3 mm in diameter with a very fine mesh. The thin films can be made from metal, silicon or plastic but the most useful is probably carbon. A shadow photograph is produced of the particles.

A life like photograph of the particles can be produced using a scanning electron microscope which work on a different principle and has a much lower resolution, in the order of microns. The electron beam is passed between tapes which cause it to scan faster in a similar way to a Television cathode ray tube. When a beam strikes a surface low energy secondary electrons are emitted and collected their intensity is displayed on a cathode ray tube which is scanned in synchronisation with the electron beam scan. In this way a complete picture of the target is built up.

2.4.2 Optical

This section is intended to cover the optical methods of sizing commonly used other than microscopy.

2.4.2.1 Particle Counting

When a particle passes through a light beam it scatters light, the intensity of which is a function of the particle size. For particles larger then about 2 μm this intensity is approximately proportional to the particle surface area but as the size falls the effect

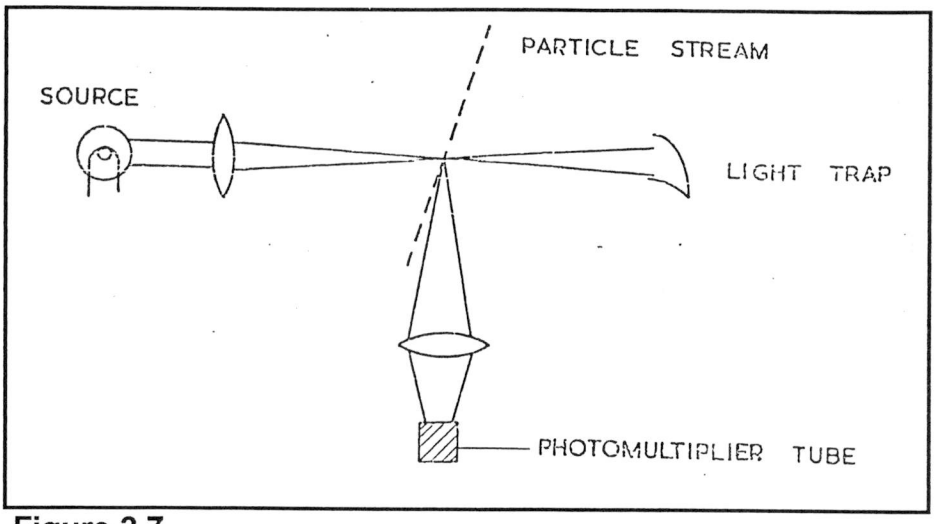

Figure 2.7

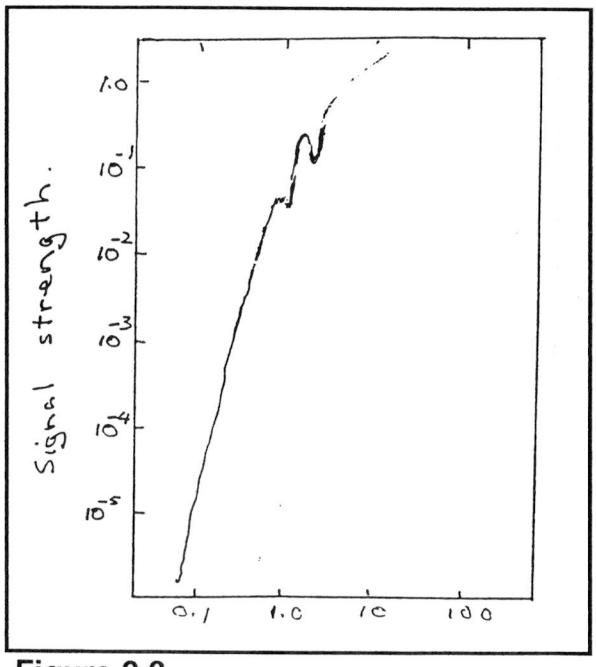

Figure 2.8

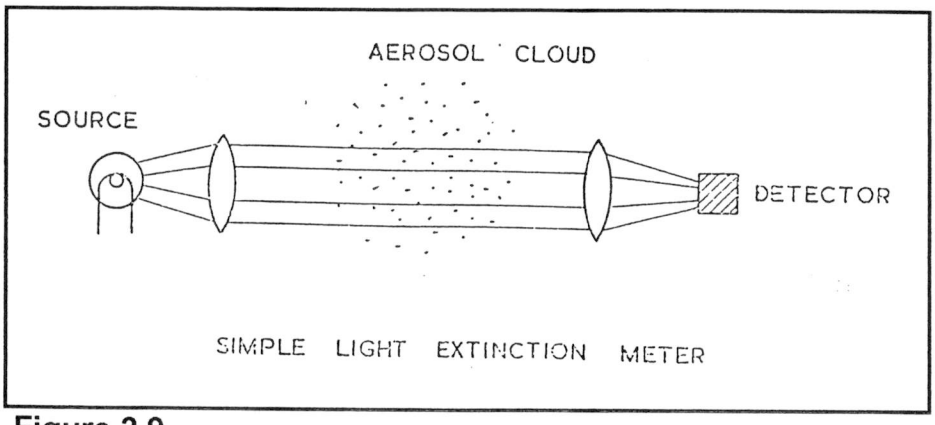

Figure 2.9

particle suspended in a gas. The particle refractive index, wavelength of incident light and particularly the angle of the scatter also effect the signal.

One of the first and simplest instruments for using this principle is shown in figure 2.7. A beam of light is focused to a point through which the particles are passed individually in a sheath of clean air. Scattering light is picked up at an angle of 90 to the incident on the photomultiplier tube. The resultant pulse is a function of size. Modern instruments use near forward scatter since the signal is stronger at this angle and a solid sate detector is often used instead of a photomultiplier tube. The lower limit on the particle size which can be measured is imposed by the signal to noise ratio which can be achieved in practice. Use of laser cavity systems in which the particle is fed through the cavity of the laser itself and in which a very high intensity and hence scattered beam is achieved has led to the extension of the lower limit to about 0.06 μm.

A typical calibration curve is shown in figure 2.8. Interpretation is difficult in the range 0.7-1.3 μm. A signal to noise ratio satisfactory for the analysis of 0.5 μm is quite easy to obtain and a wide range of instruments which count particles in the range 0.5-5 μm are on the market; they are used for clean air monitoring.

A severe restriction with these techniques is that the particle must be counted and sized one at a time -i.e. no more than one particle can be in the sensing zone at the time; hence they can only be used in a low concentration situations or with very low sampling rates [20].

2.4.2.2 Cloud Behaviour

Light attenuation (figure 2.9) is used to monitor chimney stacks emissions but is does not give information on particle size. The diffraction pattern from a cloud does contain sufficient information of this principle. They are particularly useful for analysing sprays with particles in the range of 2-1000 μm.

2.4.3 Inertial Classification

One of the most important methods for collecting and analysing samples of respirable dust is the inertial impactor. The principle of the method is shown in figure 2.10. The aerosol is passed through a small orifice directly onto a plate, or slide, which is placed at right angles to the gas flow. Particles with sufficient inertia will impact on the plate whereas those of a smaller size will be passed to the next stage of the unit with the gas stream. By operating the system as a cascade in which the jet diameter progressively reduced then successively smaller particles can be removed. The amount collected on each stage is measured. Piezo electric mass monitoring crystals have been used as impaction stages in one instrument. There are extremely sensitive and a rapid automatic output is obtained.

2.4.4 Mobility Analysis

Gravity, centrifugal and electrostatic forces to cause particle migration, and since migration velocity is a unique function of particle size, measurement of this can provide a suitable method of analysis.

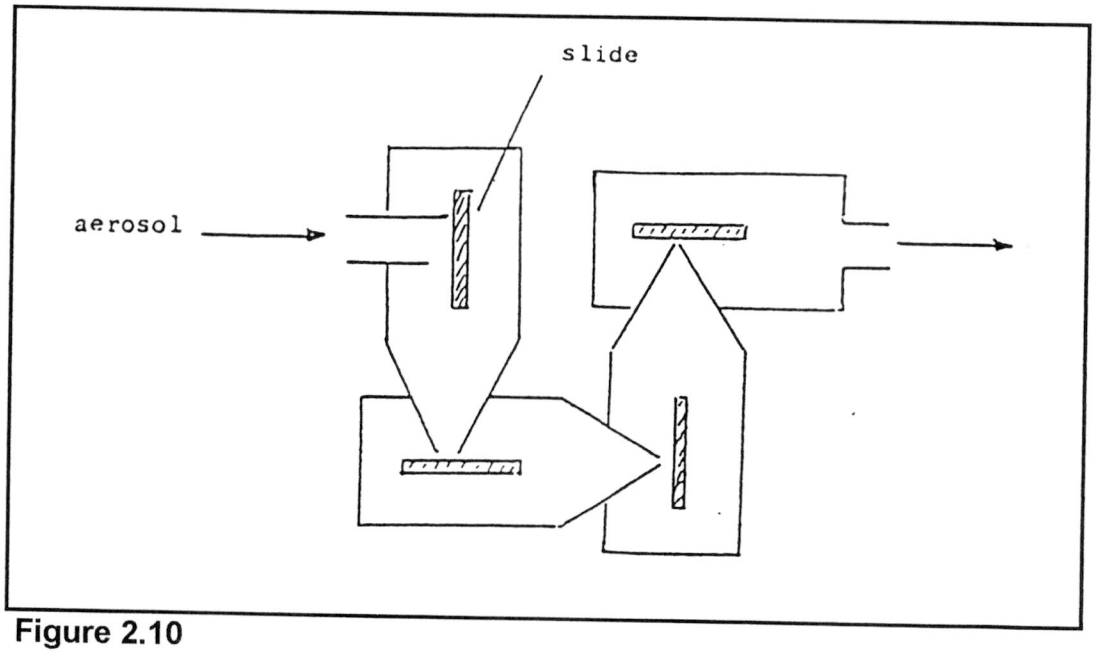

Figure 2.10

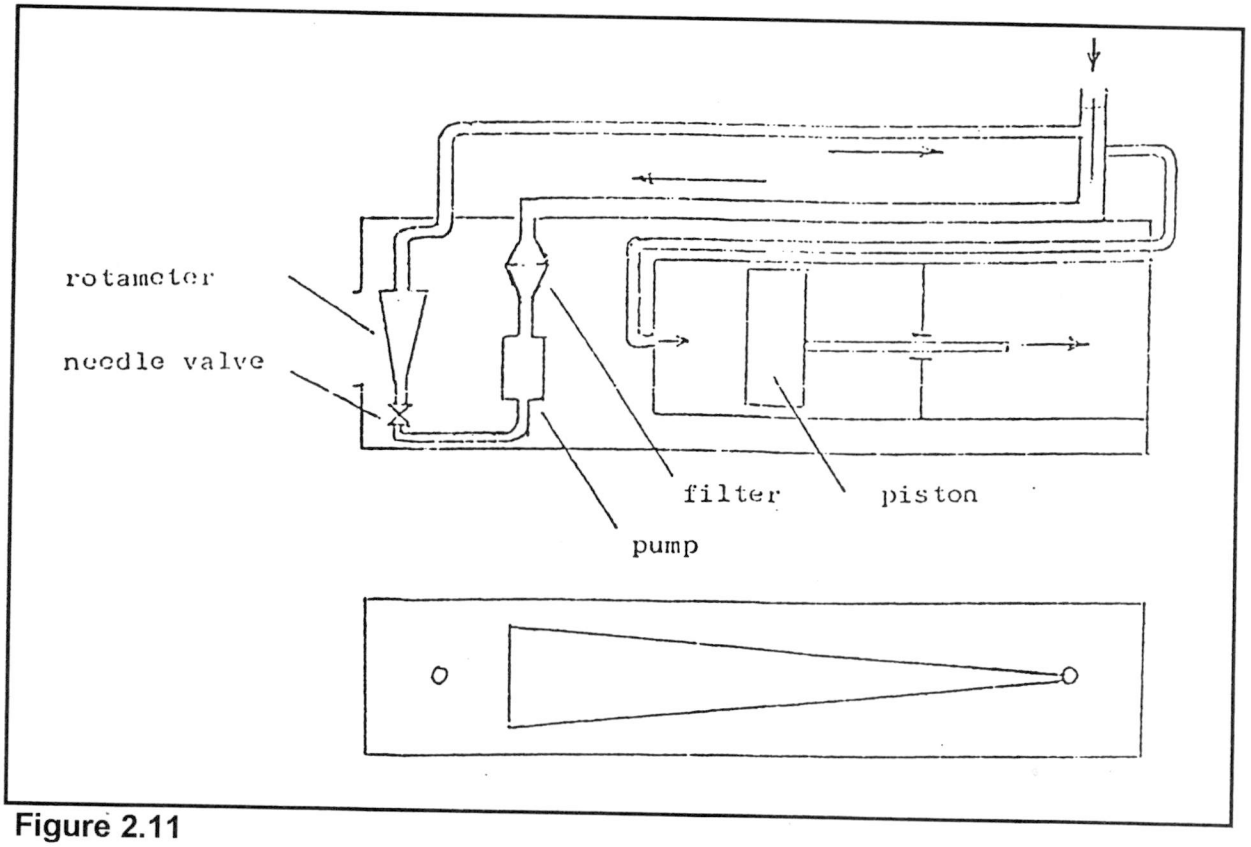

Figure 2.11

2.4.4.1 Gravitational Mobility

In the Timbrell sampling equipment (figure 2.11) the particles carried by the sample air are deposited in a size array from 1 to 100 μm in a horizontal classification channel. Clean, filtered air is circulated round the instrument by a pump at a constant rate. The size separation section is a fan shaped channel of a rectangular section. Dusty air is drawn into the instrument by a clockwork operated pump at a constant sample flow. The recirculated air and the sampled air mix before entering the separation section at the narrow end. The dust particles then settle onto six microscope slides laid end to end in a recess along the centre-line of the channel.

The distance from the apex at which a particle is deposited depends on the horizontal velocity of the air and the terminal velocity of the particle under gravity. After calibration with known spheres, the equivalent Stoke's diameter of an irregular particle can be determined from its position, and the number distribution by microscopy. The quality of the size separation appears to be good, but the usefulness of the instrument is limited to some extent by the maximum size of only 1 μm which it collects at its low sampling rate.

2.4.4.2 Electrical Mobility

If particles are passed through a charging zone in which there is a high concentration of unipolar ions they will subsequently exhibit an electrical mobility in a charged field. Diffusion charging is dominant for particles less than 1.0 μm and field charges for those greater than 1.0 μm. Hence there is a minimum in the mobility less then about 1.0 μm. Classification according to mobility forms the basis of this method of sizing.

In the electrical mobility analyser the particles are passed through a diffusion charging zone where the charge acquired is a function of their size. The aerosol is then passed into an annular precipitator (figure 2.12). In the integral size the particles of lower mobility which escape are caught at a later stage on a master filter where their total charge, and hence quantity is measured. By altering the charge on the central collection electrode the threshold level is altered so that a complete size distribution is obtained. With particles above about 0.5 μm the mobility is not sufficiently sensitive to size. With very fine aerosol the fraction of particles of a given size which are actually charged is so small so a large correction factor is required (about 99% of the particles at 0.01 μm diameter are not charged). Commercially available instruments in a complete automatic form are used for sizing aerosols in the range approximately 0.01-1.0 μm.

2.4.5 Diffusion

Fine aerosols deposit on surfaces because of Brownian diffusion. Since the diffusion coefficient, D, is related to the particle size by the Stokes-Einstein equation:

$$D = \frac{kTC_H}{3\pi\eta d_p} \qquad (2.7)$$

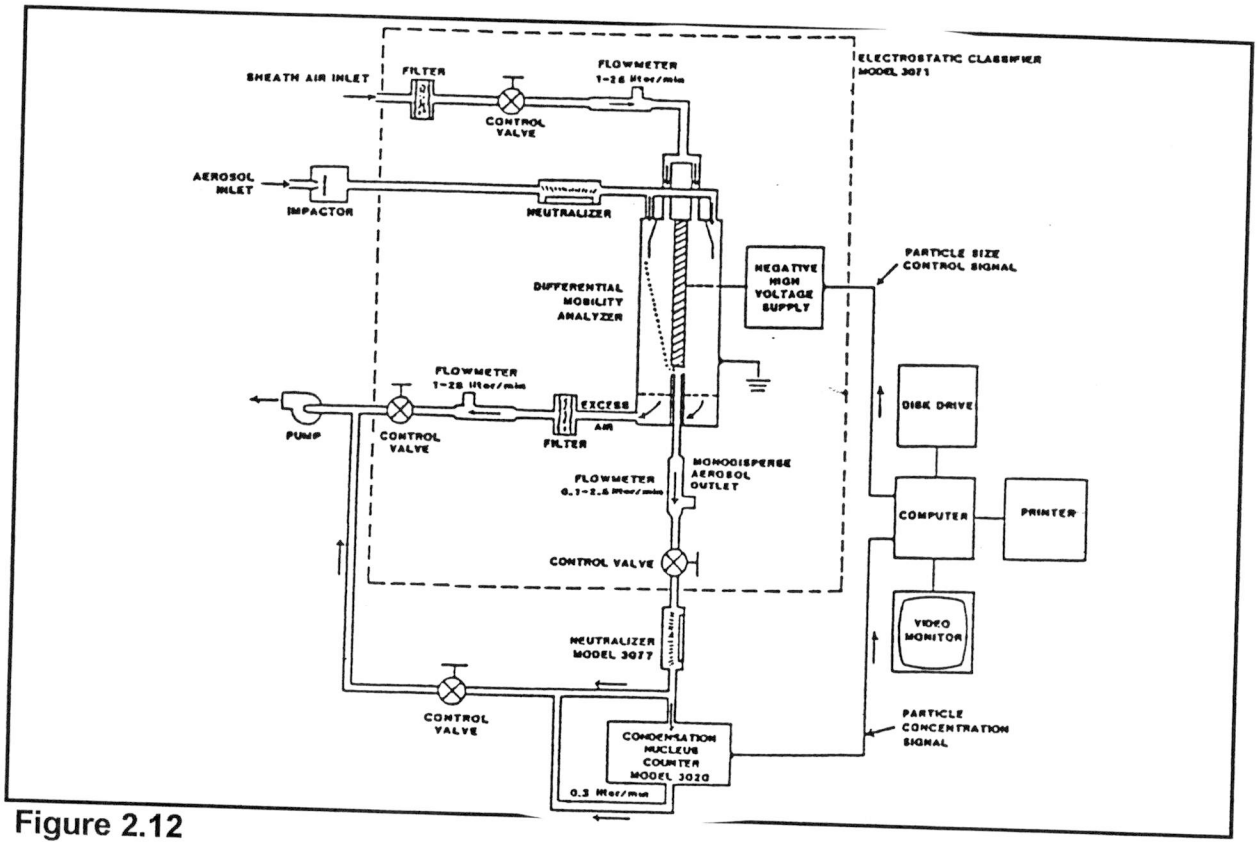
ELECTROSTATIC CLASSIFIER
MODEL 3071
SHEATH AIR INLET
FILTER
FLOWMETER
1-26 liter/min
CONTROL VALVE
AEROSOL INLET
IMPACTOR
NEUTRALIZER
DIFFERENTIAL MOBILITY ANALYZER
NEGATIVE HIGH VOLTAGE SUPPLY
PARTICLE SIZE CONTROL SIGNAL
FLOWMETER
1-26 liter/min
EXCESS AIR
PUMP
CONTROL VALVE
FILTER
FLOWMETER
0.1-2.5 liter/min
MONODISPERSE AEROSOL OUTLET
DISK DRIVE
COMPUTER
PRINTER
CONTROL VALVE
VIDEO MONITOR
NEUTRALIZER MODEL 3077
CONTROL VALVE
CONDENSATION NUCLEUS COUNTER MODEL 3020
0.3 liter/min
PARTICLE CONCENTRATION SIGNAL

Figure 2.12

It is clear that the extent of diffusal deposition can be used as a measure of aerosol size. As a flow is passed through fine capillaries or a series of grids the smallest particles are removed first. Diffusion batteries are used for the size range of 0.002-0.2 μm. They require sophisticated data reduction and do not have a high resolution but they do have the merit of measuring fundamental property. Samples are taken at progressive intervals through the device for separate concentration measurements. For this latter purpose a continuous condensation counter can be used. Particles greater than 0.4 μm tend to be removed by gravity and impaction.

2.4.6 Aerodynamic Particle Sizer.

In the APS 33 instrument (figure 3.6) the principle of particle lag is accelerating flow is used. The aerosol is rapidly accelerated through an orifice and the velocity with which individual particles leave is measured by two spot laser velocimetry. The velocity of efflux of fine aerosols will be close to that of the suspending gas stream but, because of their inertia, aerodynamically large particles will be ejected at a lower velocity. The system is completely automatic and operates at in the aerodynamic diameter range of 0.5-15 μm. Since the inertial mechanism is the most important for aerosols about 0.5 μm this is a very relevant technique [21].

2.4.7 Condensation

In a supersaturated atmospheric vapour condenses on the surface of particles which are greater than the size described by the Kelvin equation. A well known method is to supersaturate an aerosol sample by rapid adiabatic expansion. Condensation will then take place on nuclei greater then about 50 A which rapidly grow to about 5 μm diameter regardless of their initial size. The number concentration of the mist is then measured optically. N-butyl alcohol is used to create the supersaturated atmosphere in the continuous C.N.C. (figure 17). The aerosol is passed through an alcohol saturated felt lined tube and then cooled at 10°C in a chilled tube. Droplets can be counted individually for low concentration metering or by attenuation for high concentrations.

2.4.8 Mass Monitor

In the mass monitor a small electrostatic precipator is used to deposit particles on the surface of a quartz piezo-electric crystal. The crystal forms part of a resonant circuit whose frequently is controlled by its mechanical resonance. This frequently is altered by the presence of very small quantity of dust on the crystal surface hence by measuring the frequency shift a measure of the weight of deposited particulates obtained. The instrument is used for particles in a size range of 0.01-20 μm.

2.4.9 Attenuation of Sonic Waves

If a sonic wave passes through an aerosol the heat and impulse transfer between the particles and the surrounding gas causes an attenuation of the wave. The theory for this leads to an integral relation between the frequency dependent attenuation coefficient $\alpha(\omega)$ and the probability density function N(r) of the particle radius, according to formula 2.8.

$$\alpha(\omega)=\int_a^b N(r)\cdot K(\omega,r)dr \qquad (2.8)$$

with $K(\omega,r)$ a kernel function.

Vanck [22] has shown an advanced inversion technique for such a Fredholm integral, using a modified non-linear iterative method. The determination of the particle number distribution from 10 sonic attenuation measurements in the size range of 0.1 to 10 μm is shown by Beckord [23]

2.5 Review and Discussion of Condensation Type Aerosol Generators

2.5.1 Introduction

The objective of this section is to review methods used to obtain monodisperse aerosols by condensation. In general, a continuous aerosol generator produces monodisperse particles by evaporating a material and then condensing that material onto condensation nuclei in a carrier gas flow. Four, not necessarily separate, progresses are common to all such generators:

a) Nuclei production
b) Vapour generation
c) Vapour nuclei mixing
d) Condensation through controlled cooling of the carrier

Physical concerns in the operation of these processes are:

a) Short-term stability
b) Long term stability
c) Product monodispersity and reproducibility
d) Process design simplicity

2.5.2 Sinclair-LaMer Aerosol Generator

The first continuous flow monodisperse aerosol generator was described by Sinclair and LaMer [24] in 1949, and was developed during World War II. It was first used as a means of verifying the Mie Theory of electro-magnetic light scattering by small spheres [25]. In the generator as shown in figure 2.5, liquid is heated in 2 litre boiler flask under thermostated control. Filtered air or nitrogen enters a nuclei generator section, and transports nuclei across the liquid surface.

Optionally, more filtered gas may be bubbled up through the liquid, enhancing vapour production and also producing spray droplets. This gas mixture of vapour, nuclei an droplets enter the reheater, which is at a temperature about 40 to 100°C greater than of the reboiler. The droplets evaporate, and the vapour-nuclei mixture passes into a condenser tube chimney where the vapour condenses on the nuclei and the chimney walls. The entire boiler and reheater are installed in an insulated box which may take as long as six hours to thermally stabilise after start-up.

Theoretically, as shown in Wilson and LaMer [26], the aerosol should grow by diffusion of the vapour to the nuclei surface at a linear flow rate with time:

$$d_p^2 = d_0^2 + bt \qquad (2.9)$$

where b is a constant related to the vapour initial concentration and the diffusion coefficient.

Particle diameter for condensation aerosol generators dictated by a ratio of the initial vapour concentration (c_0, (kg/m^3)) to the nuclei concentration (n, (m^{-3})) in a relationship with average particle diameter:

$$d_p = \left(\frac{6c_0}{\pi \rho_p n} \right)^{1/3} \qquad (2.10)$$

with d_p , particle diameter, (m)
ρ_p , particle density, (kg/m^3)

Particle concentration is ideally limited by nuclei concentration and nuclei size distribution.

Because of the nature of equations 2.9 and 2.10, the particle size output of the Sinclair-LaMer generator is usually correlated to boiler concentration and nuclei concentration. Because of the instabilities of this process, it is often necessary to do this correlation each time the device is started up [27]. Also, if the liquid in the boiler is not replaced periodically, degradation through oxidation can occur giving unstable vapour products and a decrease in monodispersity. This can be minimised though the use of nitrogen or helium in place of air as the carried gas.

Muir [28] extended the condenser table chimney downward rather than upward after Wooding [29].This eliminated some convective mixing and solved the problem of condensate dripping back into the reheater causing bursts of instability.

Many different nuclei sources have been employed with the Sinclair-LaMer generator: tungsten and gold electrode spark generators, sublimation of salts (NaCl and AgCl) on hot plates or hot wires which condense into nuclei, and particles resulting from drying of nebulized aqueous solution sprays. In all cases, the stability of the output aerosol is greatly affected by the nuclei concentration stability and reproducibility. Because of electrode erosion and the reaction with the carrier gas, electrical nucleation source electrodes need to be continually adjusted or replaced, and nuclei concentration varies considerably between experiments. Sublimation and condensation of hot salts to produce nuclei demands a curing or training period, sometimes for days to achieve stability, and then the nuclei generator must be left on continuously until the salt source depletes as described in Huang et al [30]. The employment of nuclei from dried aqueous spray solutions as presented in Smaldone et al [31] gives an instant on capability to nuclei production, but the nebulizer stability needs to be monitored carefully.

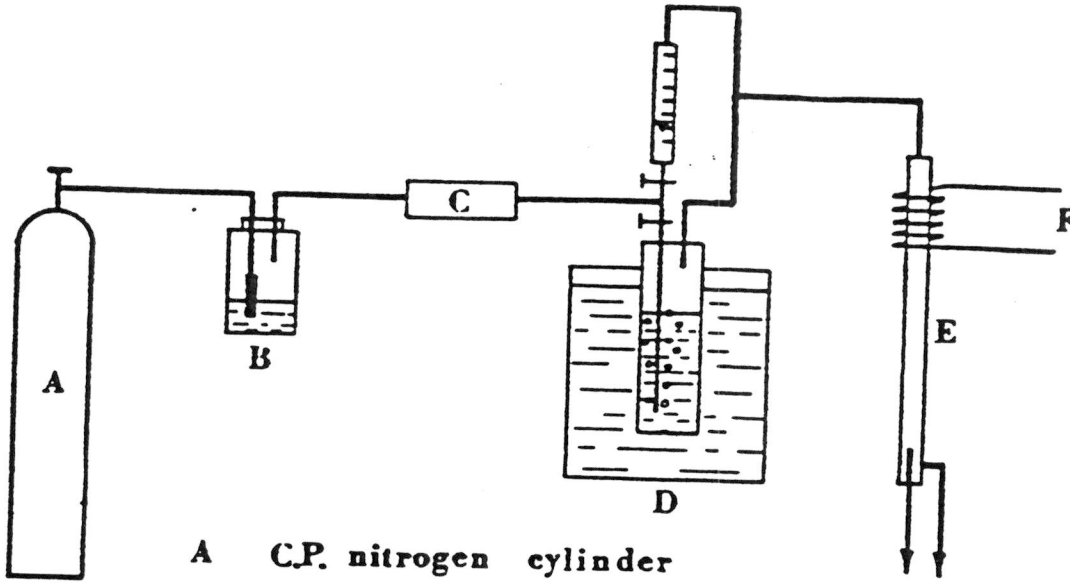

A C.P. nitrogen cylinder
B Collison generator
C Desiccator
D Thermostated bath
E Reheater
F 250 Watt heating tape

Figure 2.13

Perry and Smaldone [32] studied the use of nebulized nuclei and found no difference in their use over other sources of nuclei. Nebulized nuclei may also be chemically or radioactively labelled for long inhalation studies.

One item dealing with nuclei stability which should be of concern in the coagulation stability of nuclei with changes in reheater and boiler temperatures since high number concentration of very small particles coagulate readily at elevated temperatures.

Swift [33] conducted a series of experiments using nitrogen carrier gas, a downflow condenser chimney, no bubbling, and a low flow rate of 500 cm^3/min. rather than the more standard 2000 cm^3/min. A simple particle size-vapour pressure relationship was found for dioctyl sebacate. In the relationship of nuclei concentration versus particle diameter at constant boiler temperature only at concentrations greater than 10^5 nuclei/m^3 was there the $n^{-1/3}$ proportionality as expected by equation 2.29. The particle diameter maximum was independent of nuclei concentration below 4e4 nuclei/m^3, a phenomena also shown at 10^3 nuclei/cm^3 by Kogan and Burnasheva [34] with their KUST generator. An explanation of this phenomena is that for a set of thermal conditions, the maximum particle size caused by nuclei concentration reduction will occur at the same time as an increase in vapour wall loss since the decreasing number of nuclei near the walls can no longer deplete the vapour concentration at the walls.

Swift [33] also examined the condensation results of the use of different nuclei materials produced by sparking and by elevated temperature sublimation. Monodispersity was found to be the best when the nuclei were chemically similar to the condensing vapour species.

Huang et al [30] produced an improved version of Sinclair-LaMer generator with a smaller boiler, helium carrier gas, better thermal control, no bubbling and the use of thermally sublimated and condensed silver chloride nuclei. An upward condenser tube was located directly above the liquid in the boiler. A reheater tube and another re-condenser were located downstream from the primary condenser, which greatly improved the aerosol monodispersity. This device has been to produce linolenic and octanoic acid aerosols of diameter between 0.3 and 1.3 μm with GSD less than 1.15.

Okada et al [35] using sparked gold nuclei and an upward reheater-condenser tube produced dioctyl phthalate (DOP) aerosols of high monodispersity of diameters between 0.3 and 1.0 μm. An empirical relationship of particle diameters versus boiler temperature was used to derive the heat of vaporisation off DOP.

2.5.3 Prodi Aerosol Generator (MAGE)

Prodi [36] succeeded in making solid monodisperse particles of paraffin wax and carnauba wax with a device (figure 2.13) in which sodium chloride nuclei produced via nebulization with nitrogen (B) were bubbled though melted wax in a constant temperature boiler (D). The 0.22 to 2.2 μm diameter particles were regulated by bubbler flow, boiler temperature and vapour flow dilution. The vapour flow was routed into a reheater-condenser tube which improved the monodispersity.

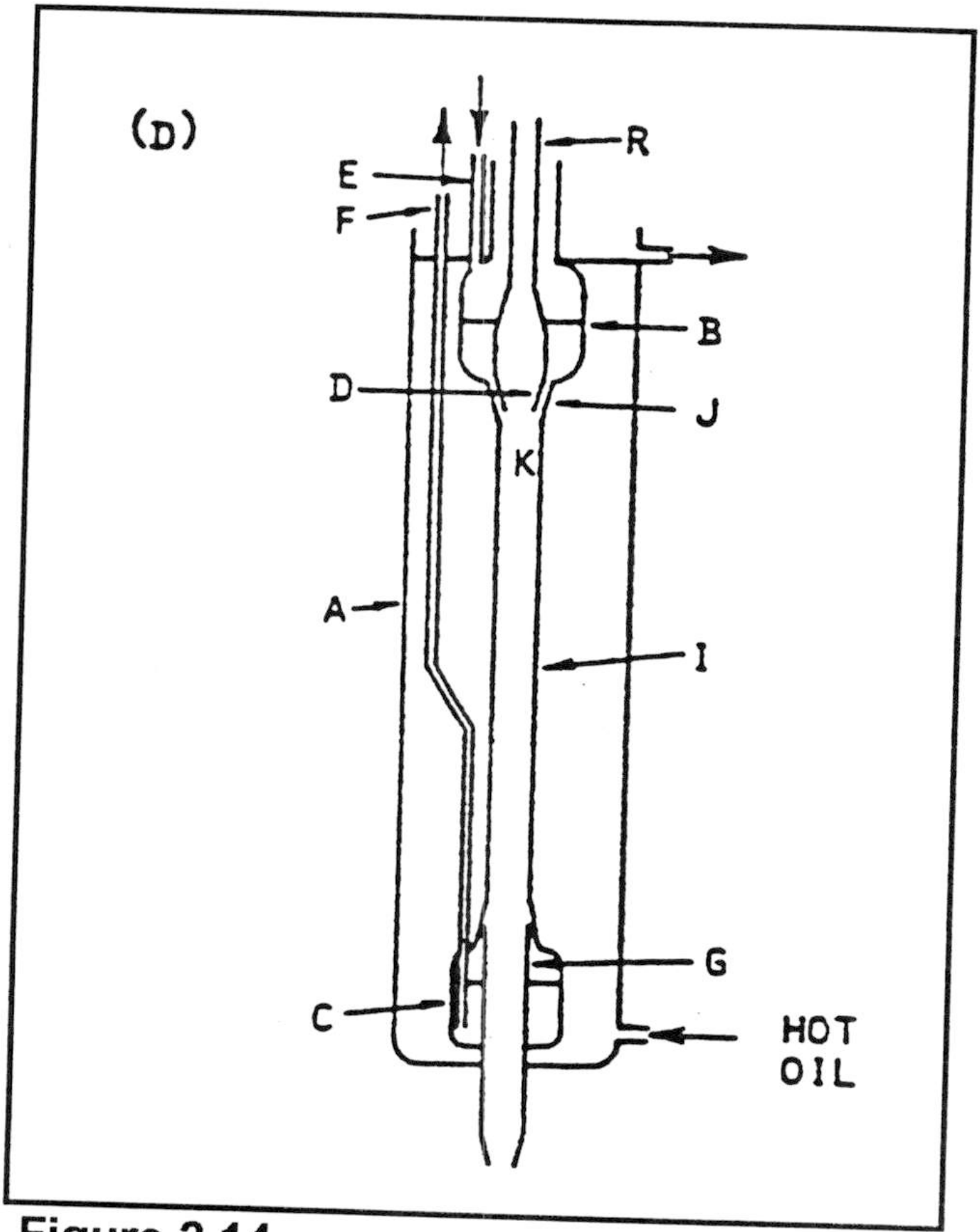

Figure 2.14

Monodispersities of 1.02 to 1.13 were measured and are quite remarkable considering that both carnauba wax and paraffin wax are mixtures of compounds, not pure compounds. This contradicts Fuchs and Sutagin (21) who stated that monodispersity is very much impaired when using condensates of low purity. However, there is no reason why mixtures of higher molecular weight substances with like boiling points and low diffusion coefficients should not condense uniformly as if they were a pure substance.

2.5.4 Falling Film Aerosol Generator

Nicolaon et al [37] and Kerker et al [38] described an aerosol generator operating under the same general principles as the Sinclair-LaMer generator, but with a much better stability and reproducibility. The falling film generator, as shown in figure 2.14, has a boiler and a reheater on a single vertical glass tube immersed in a hot oil bath. Furnace sublimated sodium chloride nuclei-laden helium enters the boiler section (D) in fully developed flow, is saturated with vapour passing through the boiler (I), exits at the end of the evaporator tube and enters a cooled condenser section (not shown). The liquid to be vaporised is fed into the boiler from the reservoir of a fixed head or height of the liquid (B), flows down into the wall of the boiler tube from a fixed gap (J) as a thin film travelling at the same speed as the carrier gas maximum velocity. The liquid is then recycled back to the reservoir. Since the liquid residence time is short, decomposition is minimised. The vaporisation zone is well defined, but care must be taken in the control of the liquid flow and the maintenance of the vertical attitude of the tube. Shahriari et al [39] simplified the generator by the use of saturated blotting paper in place of the falling film, eliminating the need for a recirculation pump, which they also claimed improved the reproducibility of the aerosol.

Nicolaon et al [40] studied the effect of the reheater section downstream of the condenser tube. The reevaporation of the aerosol and the subsequent recondensation greatly improved monodispersity: GSD improved from 1.17 to 1.08. Samples where taken from the centre of the parabolic condensation profile and where more monodisperse than samples taken from the sides. The aerosol condensation profile almost exactly fit a numerically generated heat transfer temperature profile calculated at the same dynamic conditions. Aerosol sampling downstream of the condensation zone showed that the particles were fully condensed 0.3 seconds (approximately 2 cm) from the initiation of the condensation and obtained 94% of their diameter within the first 0.1 seconds (0.66 cm) after condensation initiation.

Nicolaon and Kerker [41] Further studied that the rates of cooling increase, supersaturation increases and smaller, previously inactive nuclei of a polydisperse nuclei distribution become active, reducing the end product aerosol particle size. Liao [42] suggested that higher cooling rates produce a more monodisperse aerosol, agreeing with the observation of Nicolaon and Kerker [41].

2.5.5 Q127 HOT DOP Aerosol Generator

The Air Teqniques Incorporated Q127 Aerosol generator has been in use for over the thirty years as a particulate source for filter testing. It is similar to the Sinclair-

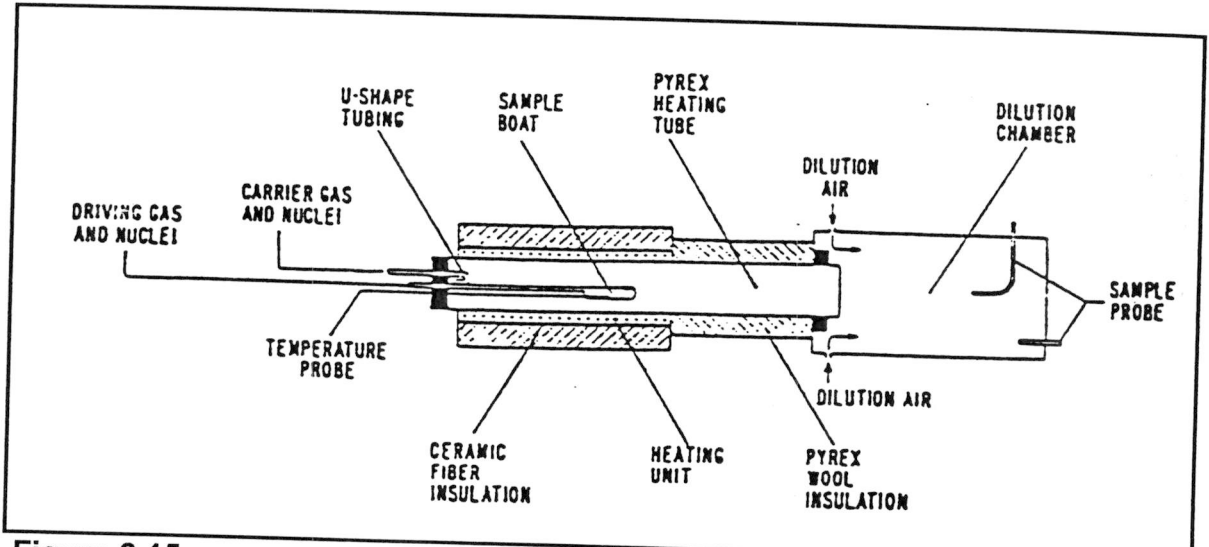
U-SHAPE TUBING
SAMPLE BOAT
PYREX HEATING TUBE
DILUTION CHAMBER
DILUTION AIR
CARRIER GAS AND NUCLEI
DRIVING GAS AND NUCLEI
SAMPLE PROBE
TEMPERATURE PROBE
DILUTION AIR
CERAMIC FIBER INSULATION
HEATING UNIT
PYREX WOOL INSULATION

Figure 2.15

LaMer generator in that hot filtered air enters a canister holding a pool of hot dioctyl phthalate liquid. No reheater or nuclei source exists. The vapour-laden air passes through a pipe junction where it is mixed temperature controlled diluent air and becomes supersaturated. Homogeneous nucleation results and the end product in an aerosol of diameter between 0.24 and 0.28 μm with GSD less then 1.2 as reported by Hinds et al [43]. Because of the use of air as carrier gas, dioctyl phthalate Thermal decomposition in the boiler can be significantly widen the GSD Over a period of time throw of the calibration of the single angle (90°) polarisation sizer (OWL). Hinds et al [43] showed that particle size was adjustable from 0.205 to 0.3 μm by changing the diluent air temperature.

2.5.6 Tu Single Stage Condensation Aerosol Generator

Tu [44] described a simple single stage condensation aerosol generator as shown in figure 2.15. Nuclei-laden driving gas enters a sample boat containing the hot aerosol liquid or melded solid and exhausts into a heated horizontal glass tube. More of the carrier gas-nuclei mixture enters upstream of the sample boat and, combining with vapour flow, moves down the tube into an insulated, but unheated condenser section. The mixture is slowly cooled, condensation takes place and the aerosol enters the dilution chamber where it is mixed with clean filtered air. Only a small, replaceable amount of aerosol source material is used (15 g), so that decomposition is avoided.

Particles have been made of carnauba wax, stearic acid an many other organics. Diameters have been produced between 0.1 and 2.0 μm with GSD between 1.06 and 1.18.

The condenser heat transfer is horizontal mixed convection with the majority being free convection. The face velocity is very low. The temperature profile in the condenser is controlled by the insulation, and is probably that just after condensation is complete, the aerosol exists and is diluted. The insulation is very important, for without it is a sharp drop in the temperature profile would greatly decrease monodispersity. Changes in particle size in this generator are a balance of vaporiser temperature, carrier and driving gas flow balances and nuclei concentration.

2.5.7 Kogan-Burnasheva Aerosol Generator

Kogan and Burnasheva [45] described a mixer aerosol generator (often called KUST apparatus) in which a cold gas nuclei mixture (C) and a hot, vapour-laden gas from (A) flow together into a mixing nozzle (B) as shown in figure 2.5. The hot gas passes through the porous grains of silica gel (A), impregnated with the liquid to be vaporised. Particles grow by condensation downstream of the nozzle.

In absence of nuclei, condensation occurs only at the walls, but with nuclei present monodisperse aerosols can be created. The degree of supersaturation of the mixture depends on the liquid material, flow conditions, vaporiser temperature, nuclei concentration and the mixing gap width. Nuclei less then 0.01 μm of turbine oil, dioctyl phthalate and sodium chloride have been used with success.

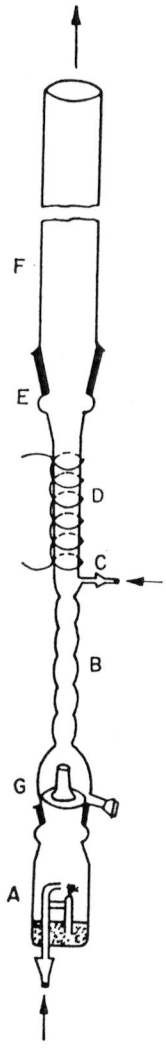

FIG. 3.

Rapaport-Weinstock generator.

Figure 2.16

Fuchs and Sutugin reported with this apparatus dibutyl phthalate aerosols of diameter between 1 to 2 μm , GSD between 1.06 and 1.12 for nuclei concentrations less than 10^4 particles/cm^3. The mean particle diameter was independent of nuclei concentration below 10^3 particles/cm^3 because of high vapour wall losses.

Sutugin [46] showed the usefulness of this device in preparing monodisperse dioctyl sebacate aerosols of diameters from 0.006 to 0.06 μm nucleated by 0.0034 μm monodisperse sodium chloride.

2.5.8 Rapaport and Weinstock Aerosol Generator

The use of a nebulizer as the source of polydisperse particles to be evaporated and subsequently condensed into monodispersed particles was first reported by Rapaport and Weinstock [47]. The apparatus as shown in figure 2.16, was very simple when compared when compared to the Sinclair-LaMer generator. A nebulizer (A) creates a spray aerosol which flows up a tube to a heated evaporation section (B) where the particles evaporate. The particle condense in the chimney (C) into a monodisperse aerosol. The aerosols were reported to be formed by homogeneous condensation, but the reported diameters of 0.92 to 1.2 μm are more indicative of nucleated aerosols.

One of the obvious advantages of the system was its instant-on vapour source and 1/2 hours quick warm-up. The residence time of the material in the evaporator is small, and thermal decomposition is almost eliminated, an advantage over generators with heated pool reservoirs.

Lassen [48] showed that placing glass wool plugs of two centimetre thickness into the tube just downstream of the evaporator, particles of 1.2 μm diameter resulted where without the glass wool, 0.8 μm particles were formed. This was taken as a proof that residual nuclei left after spray droplet evaporation were present. The distance between a baffle screen and the nebulizer varied removed larger spray particles and the changed the vapour mass concentration without an appreciable change in nuclei concentration. In this way, particle diameter was varied 0.3 to 1.4 μ m without changing the evaporator temperature with only one change to the atomiser pressure.

Preining [49] showed a version of the Lassen [48] generator with adjustable impactor plate located on the nozzle. Berner and Preining [50] reported that the nuclei left after evaporation were the result of the degree of purity of the liquid. Purer gave polydisperse aerosols, probably as a result of homogeneous nucleation. The addition to the liquid solution of a substance of high boiling point (anthracene) provided a controlled impurity from which nuclei of a controlled size could be formed.

Liu et al [51], and later Tomaides et al [52], discussed a greatly refined design of the Rapaport and Weinstock style of generator. A single orifice-Collison nebulizer (British Standards 2577 [53]) was fed with purified air to provide a stable polydisperse aerosol. A fine mesh screen provided uniform, laminar aerosol flow down into an evaporator section and finally to the condenser tube where the aerosol formed.

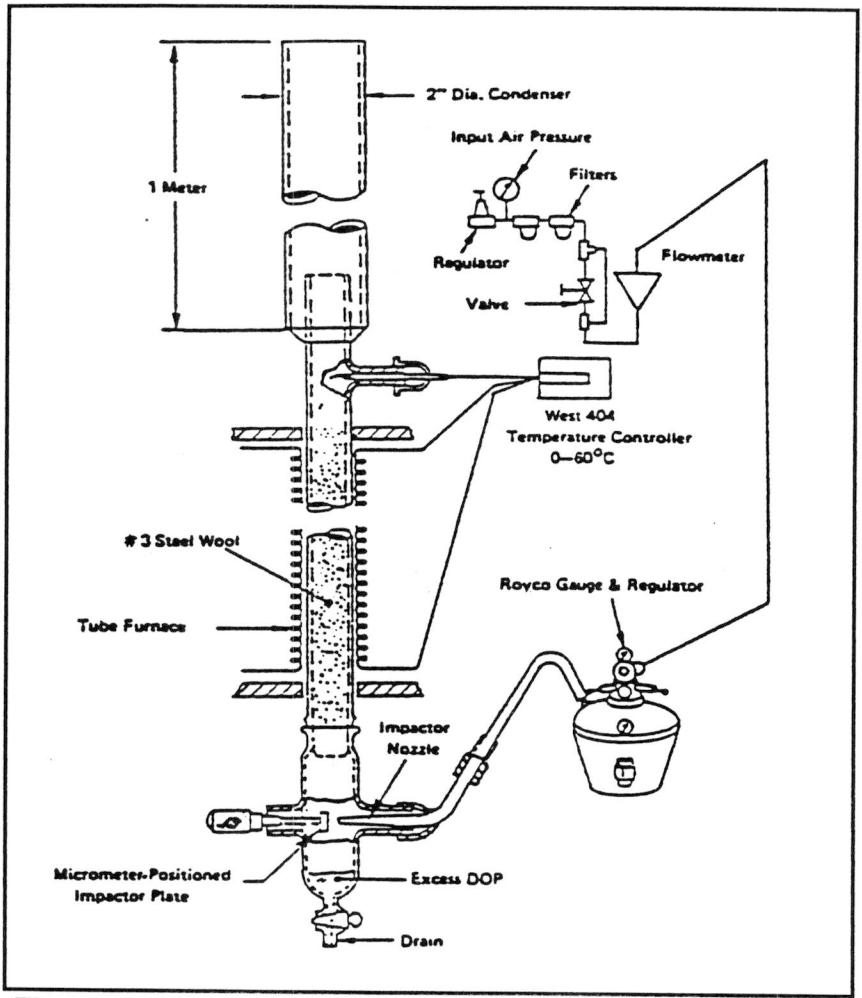
2" Dia. Condenser
1 Meter
Input Air Pressure
Filters
Regulator
Flowmeter
Valve
West 404
Temperature Controller
0–60°C
#3 Steel Wool
Tube Furnace
Royco Gauge & Regulator
Impactor
Nozzle
Micrometer-Positioned
Impactor Plate
Excess DOP
Drain

Figure 2.17

Since it was found that the monodispersity in the centre of the condenser flow profile was much better than of the total flow (GSD of 1.15 compared to 1.35), only the central portion of the tube flow was extracted for use. The temperature of the evaporator section was regulated by controlled voltage applied to heating tape. In the Tomaides et al [52] version, a shield was placed around the evaporator-condenser section to help stabilise the tube wall temperature.

In an experiment with dioctyl phthalate, the evaporator temperature was incrementally increased , and subsequently the aerosol mean diameter increased and decreased again. This indicates three regions. Low temperature where the polydisperse aerosol is incompletely evaporated, mid-temperatures where the liquid is completely vaporised, and high temperatures where the loss of nuclei due to coagulation becomes critical and the nuclei-wall vapour competition becomes unstable. Reducing the total flow greatly improved monodispersity. An electrostatic charge nebulizer was also added, since the spray particles were found to have a significant bipolar electrostatic charge.

By diluting the liquid in the nebulizer with a high vapour pressure liquid (alcohol), Liu et al [51] were able to generate aerosols of diameters from 0.036 to 1.3 μm with GSD from 1.5 to 1.14 respectively. In Tomaides [52], anthracene was added to the liquid as the impurity and the quality of the aerosol was unchanged when the anthracene mass to feed liquid volume ratio was varied from 0.1 g/litre to 1 g/litre.

Liu and Lee [54] showed that the stability of this type of aerosol generator is greatly affected by the stability of the nebulizer. They presented a nebulizer incorporating a precision orifice nozzle with a fixed impactor plate. Excess impactor-captured liquid was allowed to drain off. Constant fresh liquid feed was provided syring pump. The aerosol generator concentration output fluctuated 5% over a 60 minute period, while a collision nebuorificelone varied over 250% in 60 minutes. This greatly improved polydisperse aerosol stability gave the condensation aerosol generator a nearly constant vapour an nuclei ratio over a long period.

A.D. Little [55] experimented with several versions of the Rapaport and Weinstock generator in an effort to duplicate the aerosol produced by the Q127 HOT DOP aerosol generator. As shown in figure 2.17, a nebulized polydisperse aerosol is fed to an adjustable impactor plate which controls the aerosol mass concentration. The aerosol flows up through an evaporator packed with steel wool to enhance heat transfer, and finally enters an upward condenser tube.

The 43 litres/minute volume flow airflow output of this generator is the highest published for a Rapaport and Weinstock generator. The severe restrictions placed on the volume flow and mass concentration of this design by the U.S. military specification required theoretical Q127 performance yielded a 0.3 micrometer mean diameter with GSD between 1.13 and 1.16. The original goal of GSD at 1.10 could only be achieved at flow-rates less than 10 litres/minute and any increase in flow rate or concentration increased polydispersity.

Soderholm et al [56] evaluated the output of the A.D. Little [55] generator using a variety of materials: dioctyl phthalate, pentaethylene glycol, tetraetylene glycol

dipropionate and oleic acid. No decomposition products as monitored by gas chromatography and mass spectrometry were found at different evaporator temperatures selected to give GSD<1.3, except in the case of tetraethylene glycol dipropionate.

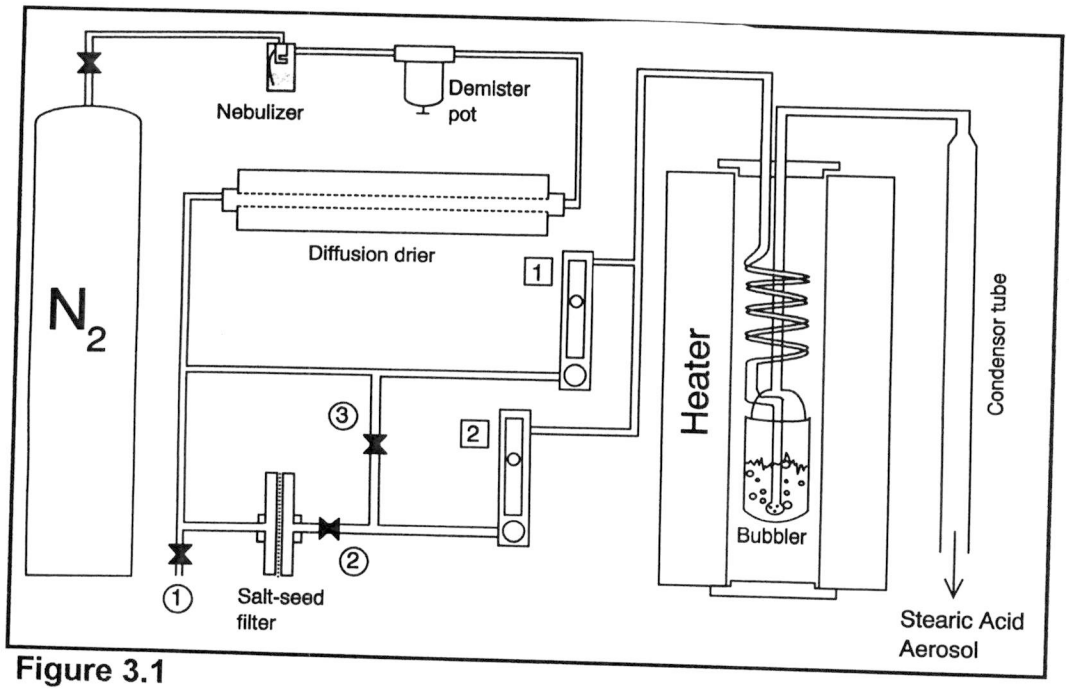

Figure 3.1

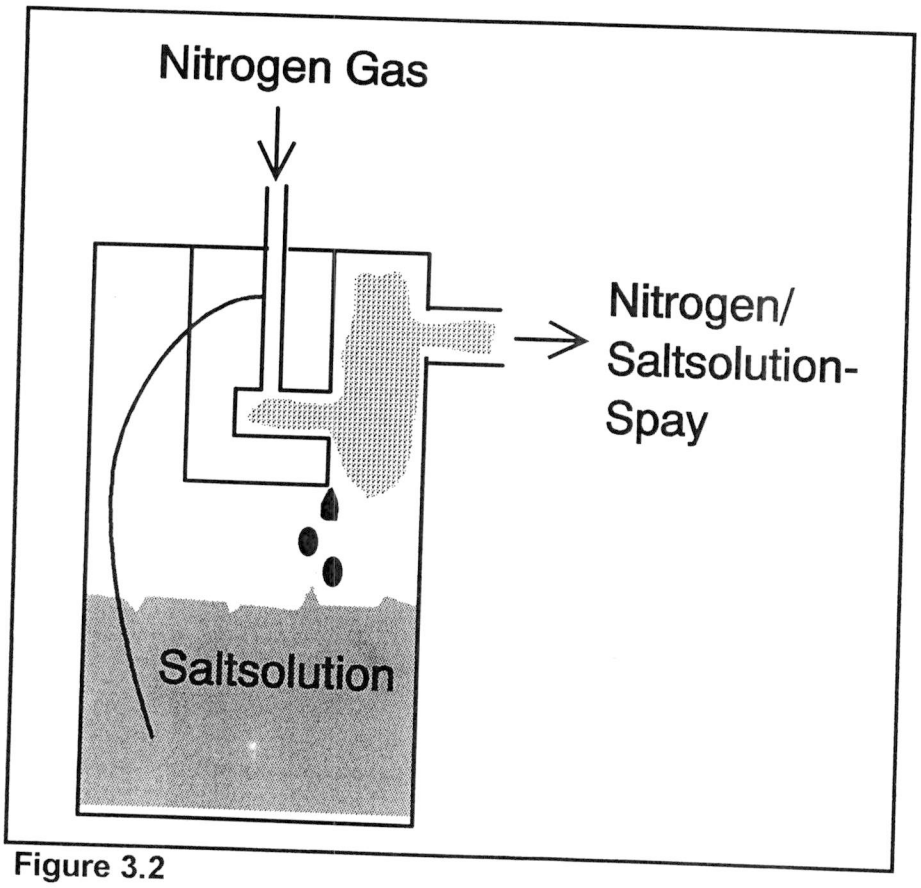

Figure 3.2

3 Experimental Apparatus

3.1 Description of the IMAGE

The experimental rig is shown in figure 3.1. In the nebulizer (fig. 3.2) a polydisperse spray is produced from a NaCl solution. Pressurised high purity nitrogen enters at the top of the nebulizer and sucks the liquid (salt solution) from the liquid reservoir via the small tube. In the nozzle the nitrogen-liquid mixture reaches a high velocity and under a pressure drop the liquid jet brakes open. Any large droplets are removed by colliding against the wall, and flow back into the liquid reservoir, while the smaller droplets enter the diffusion drier. To enhance the life of the diffusion dryer a demister pot is used to remove large liquid droplets. In the diffusion drier the salt solution spray is dried. The diffusion drier is filled with silica-gel which absorbs the water from the droplets, and a seed aerosol of salt remains. The salt-seed aerosol can directly enter the bubbler or the flow can be split and filtered, before being rejoined, to reduce the salt-seed concentration. The bubbler, which is heated by a furnace, is filled with a low melting point organic, stearic acid. In the furnace the nitrogen/salt-seed flow is heated in the spiral before it enters into the bubbler. As the nitrogen flow bubbles through the liquid stearic acid some of the stearic acid evaporates. In the condensation tube after the furnace, the evaporated stearic acid condenses onto the salt-seed particles as the temperature of the mixture falls.

3.2 Description of the Measuring Devices

3.2.1 Aerodynamic Particle Sizer

The Aerosizer's Aerodynamic Time of flight measurement technique was developed by Dr. Barton E. Dahneke. The Aeroziser particle measuring system is capable of measuring individually the size of particles in the range of less than 0.2 to 700 μm and measures particle size by expanding the air-particle suspension through a nozzle into a partial vacuum (see figure 3.3). The air leaves the nozzle at a near sonic velocity and continues to accelerate through the measurement region. Particles are accelerated by the drag forces generated by the accelerating air stream. Very small particles are accelerated to nearly the air velocity by the drag force between the air and the particles. Large particles experience lower acceleration because of their greater mass.

Force Equation

The general form of the force equation is given by:

$$C_d \frac{\pi d^2}{4} \rho_a \frac{(v_a - v_p)^2}{2} = \frac{1}{6} \pi d^3 \rho_p \frac{dv}{dt} \qquad (3.1)$$

where C_d = Drag Coefficient
ρ_a = density of the air , kg/m^3
v_a = velocity of the air , m/s

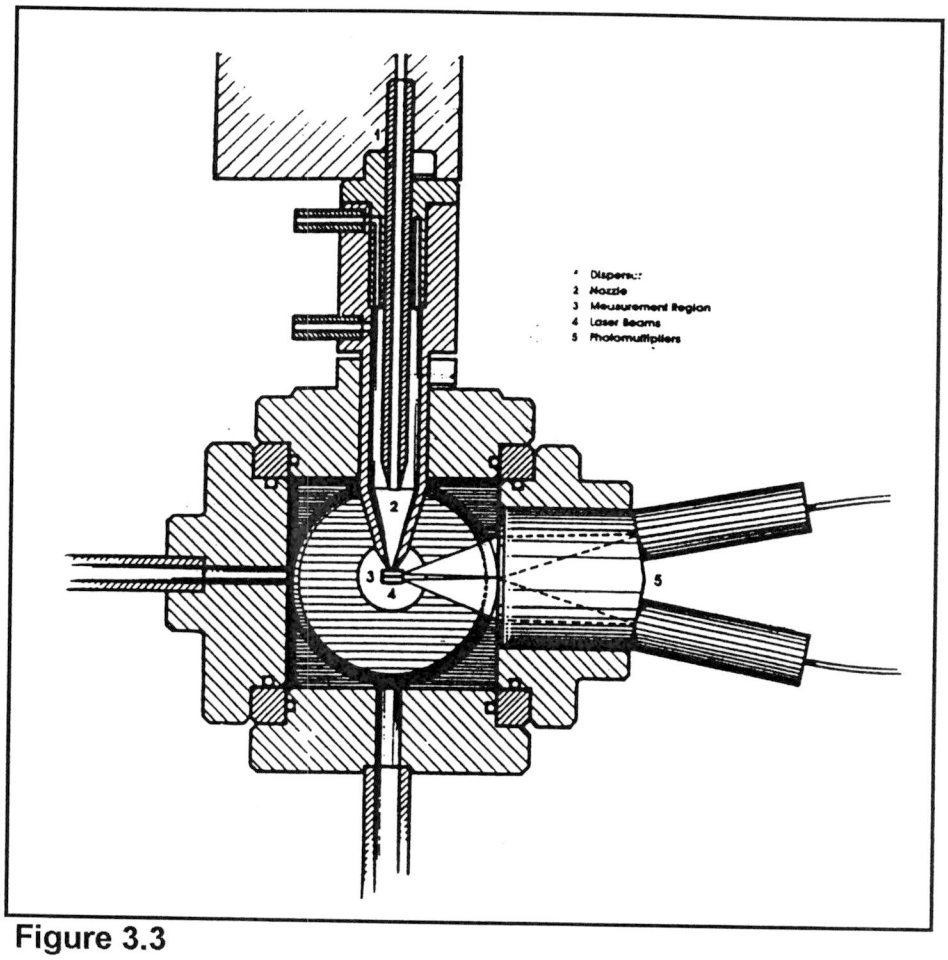

Figure 3.3

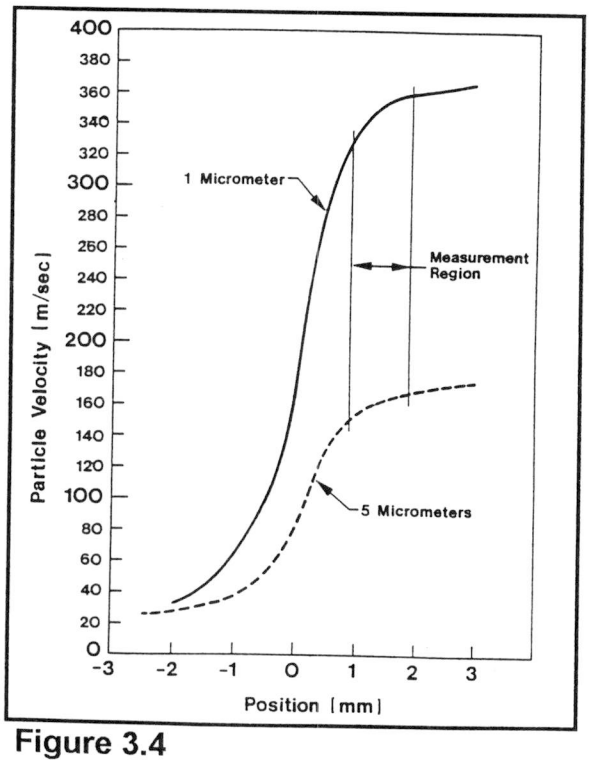

Figure 3.4

v_p	=	velocity of the particle	, m/s
d	=	particle diameter	, m
ρ_d	=	density of the particle	, kg/m^3

The $C_d \frac{\pi d^2}{4}$ term relates the drag coefficient and the projected area of the particle to the force while the $\rho_a \frac{(v_a - v_p)^2}{2}$ relates the air density and the differential velocity of the air and the particle to the force applied on the particle. The other side of equation 3.1 is simply the particle volume multiplied by the density $\frac{1}{6}\pi d^3 \rho_p$ to get the particle mass and the particle acceleration $\frac{dv}{dt}$

Particle Velocity and Size

A comparison of the velocity of 1 and 5 μm diameter particles as the are accelerated through the nozzle is given in figure 3.4. The end of the nozzle is at 0 mm. Positive positions are in the vacuum chamber while negative positions are before the nozzle exit.

Particle Size and Time of Flight

The Time-of-Flight of a single particle is measured by the generating two beams of laser light through the instrument's measurement region. As particles pass through the laser beams, they scatter light which is detected and converted into electronic signals by two photomultiplier tubes. One photomultiplier detects light scattered as the particles through the first beam. The other photomultiplier detects light scattered as the particles pass through he second beam. The time between these two events (the time of flight) is measured with a precision of 25 nanoseconds. The relationship between the particle size and the time of flight depends on the density of the particle. The relationship has been carefully determined using a combination of theoretical concepts and the experimental measurements of the particles with accurately known diameters and densities. Figure 3.5 shows the results of this determination. These results are entered into the computer program and are used change measurements of the time of flight into particle size. Only the density of the particles must be known to permit this conversion. The generated aerosol is filtered for safety reasons in a master filter.

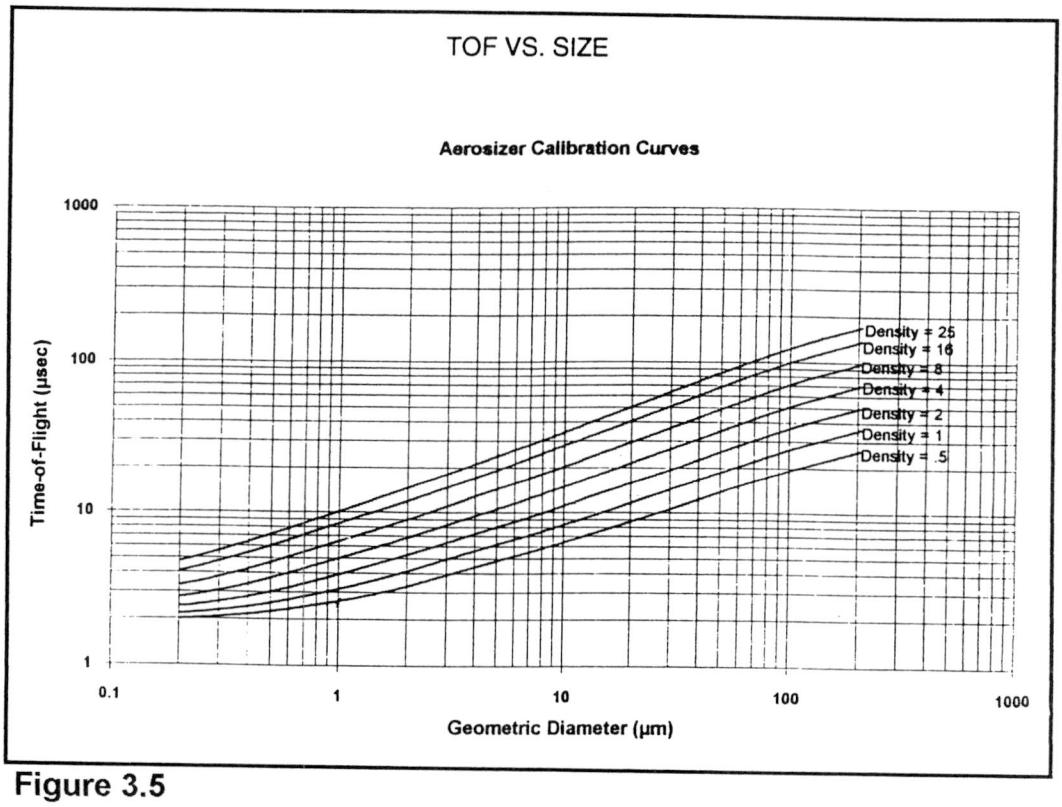

Figure 3.5

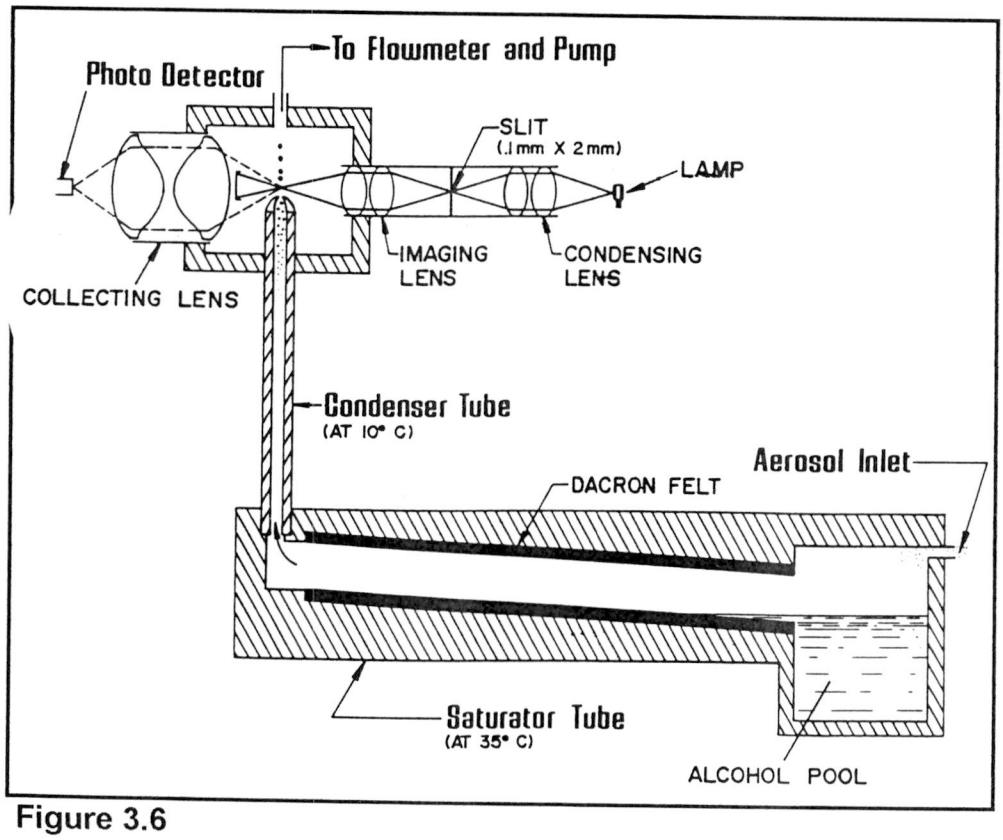

Figure 3.6

3.2.2 Condensation Nucleus Counter

The purpose of the Condensation Nucleus Counter (CNC), shown in figure 3.6, is to measure the number concentration of submicron particles. In the saturator, the aerosol flow is saturated with n-butanol. In the condenser the alcohol vapour condenses on the aerosol particle causing them to grow to droplets of about 12μm. Each droplet is large enough to scatter a detectable light beam, although the dry particle would have been much to small to be detected. The droplet size is nearly independent of the size of the original particle over a wide range of particle sizes, so the light scattered is a function of number concentration only, not of size distribution. The droplets pass from the condenser tube into the viewing volume trough a 1.0 mm diameter nozzle. In the viewing volume, the light of a halogen light bulb is scattered by the droplets within a 90° angle. Droplets can be counted individually for low concentration metering or by attenuation for high concentrations.

3.3 Explanation of Methodology

3.3.1 Collecting of the Aerosol for Size of the Aerosol

The aerosol was collected at the end of the condenser tube in a plastic basket of ca. 3 litre for about 10 seconds at an aerosol flow rate of 4.8 l/min and proportional longer to the 10 seconds for smaller flow rates. After the collection the basket was moved to the aerosizer and analysed for about 10 seconds.

3.3.2 Collecting of the Aerosol for Bubbler Efficiency Calculation

To measure the total mass of the particles in the nitrogen flow at a certain temperature, the aerosol was collected on a fibre glass filter. The filter was attatched to a vacuum pump (as shown in figure 3.7) with a flow rate bigger than the aerosol flow so that all the aerosol could be collected on the filter. The weight of the filter was measured before the aerosol collection and after a fixed measured time, using a sensitive balance.

3.3.3 Temperature Measurements for Vapour-Liquid Calculation

The temperature of the heater (temperature of the vapour liquid equilibrium) was measured with a thermometer suspended though a hole in the top plate of the furnace at the position shown in figure 3.8. During the last measurements it was shown that the temperature measured with the thermometer was to high. The correct temperature was measured with a thermocouple at the position shown in figure 3.8. The tip of the thermocouple was covered with insulation on the side nearest the furnace wall, to prevent direct heating from the furnace. In this way the actual liquid temperature was measured.

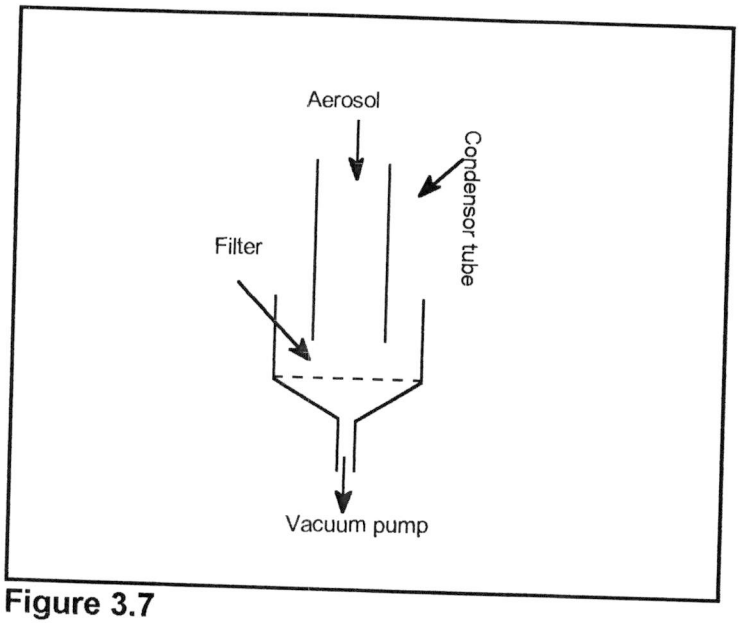

Figure 3.7

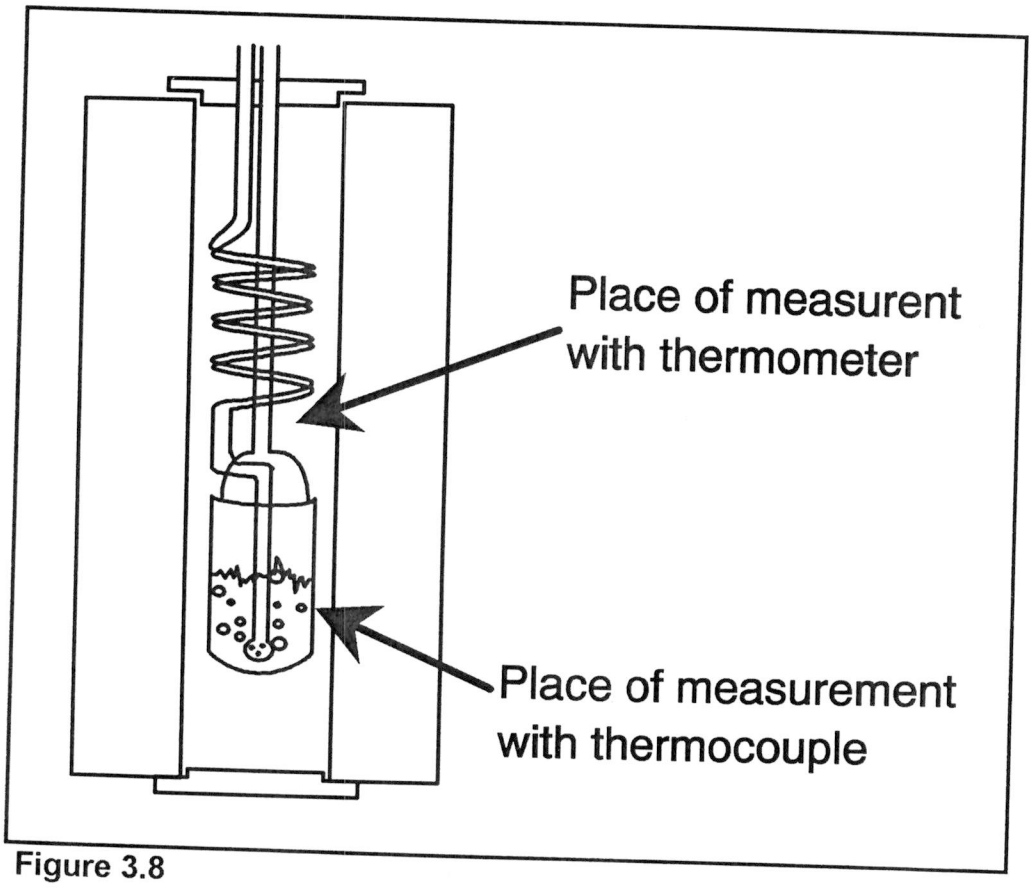

Figure 3.8

3.3.4 Salt Solution for Salt-Seed Generation

The salt solution used in the nebulizer was a sodiumchloride solution. 0.20 gram sodium chloride was mixed in 500 ml highly purified water, with an electrical conductivity of > 18 MΩ cm.

3.3.5 Stearic Acid

The stearic acid used in the bubbler was normal commercial available granulated stearic acid from the company, Fisons. The Fisons code was s/8130/53. The density was 730 kg/m^3 with a purity of 99%.

The stearic acid concentration in the vapour phase was calculated according to the ideal gas law, the concentration (g/l) in the vapour phase is given by:

$$c = \frac{P^{sat}}{RT}\frac{M_w}{1000} \qquad (3.2)$$

with	P^{sat}	vapour pressure of stearic acid	(Pa)
	T	temperature	(K)
	M_w	molecular weight of stearic acid, 284.5	(g)
	R	gas constant, 8,314	(J/mol/K)

The vapour pressure of stearic acid is calculated according to the extended Antoine equation:

$$\ln P^{sat} = 124.7 - \frac{16598}{T} - 13.56 \ln T + 3.159 \cdot 10^{-18} T^6 \qquad (3.3)$$

The coefficients of this equation are extracted from the compound database of ASPEN PLUS. Equation 3.3 is visualised in figure 3.9.

3.3.6 Heating Tape as Reheater

A 1 meter long heating tape was used with a heating capacity off 240 Watt. The heating tape was covered with fibre glass, for insulation and protection. The position of the heating tape is shown in figure 3.10. During the measurements of the bubbler efficiencies, the heating tape was extendet to the first part of the condensor tube.

3.3.7 Filter for Salt Seed Filtering

Two types of filters were used to filter the salt seeds from the nitrogen flow. First a Whatman filter paper, cat. No. 1003 090 was used and then a Whatman glass microfibre filter, type GF/B, catalogue number 1821090 was used.

When the bypass is not used, valve 3 is opened and valve 2 and rotameter 1 are closed, only rotameter 2 is used. When the filter is used, valve 3 is closed and valve 2 is opened, both rotameters are used.

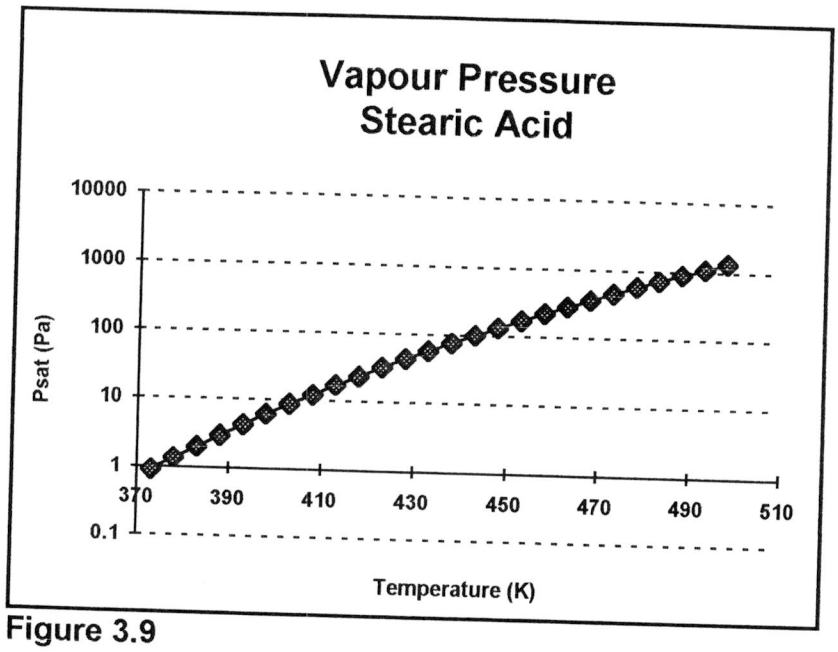

Figure 3.9

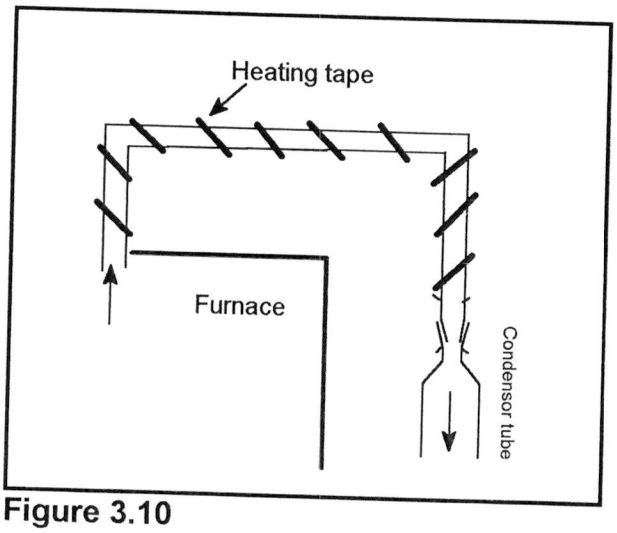

Figure 3.10

The ratio of the number concentration of the salt-seeds to the salt-seeds without filtering is given by:

$$\frac{n}{n_0} = \frac{\phi_{v,non-bypass}}{\phi_{v,non-bypass}\phi_{v,bypass}} \tag{3.4}$$

3.3.8 Furnace

The used furnace was Eurotherm thyristor. The length of the furnace is 18 inches and the diameter of the tube is 3 inches. The stability of the heater was plus minus 1°C. Stability is reached after 1 hour.

3.3.9 Preheater

The preheater was so designed that length was equal to the preheater length of the MAGE and that the preheater and the bubbler could be placed in the furnace. The total length of the glass-tube is 0.80 m with a outside diameter of 7.7 mm and a wall thickness of 1.5 mm.

In paragraph 4.7 is the heat transferred, and so the temperature rise, in preheater calculated. The tube is devided in 100 pieces. For each piece of tube, the heat flow (J/s) is calculated according to;

$$\phi_w = AU(T_{furnace} - T_{gas}) \tag{3.5}$$

with;

$$\frac{1}{U} = \frac{1}{h_{inside}} + \frac{d_{wall}}{\lambda_{wall}} + \frac{1}{h_{outside}} \tag{3.6}$$

and	A	heat transfer area	(m^2)
	U	total heat transfer coefficient	(W/m^2K)
	h_{inside}	heat transfer coefficient on the inside, 19	(W/m^2K)
	d_{wall}	thickness of the tube	(m)
	λ_{wall}	thermal conductivity of the wall, 1	(W/mK)
	$h_{outside}$	heat transfer coefficient on the outside, 10	(W/m^2K)

The temperature rise (K) in that piece is given by;

$$\Delta T = \frac{\phi_w}{\phi_m c_p} \tag{3.7}$$

with	ϕ_w	heat flow	(J/s)
	ϕ_m	mass flow	(kg/s)
	C_p	specific heat, 1.04	(J/gK)

The h_{inside} is calculated according to;

$$h_{inside} = 3.66 \frac{\lambda_{gas}}{D_i} \qquad (3.8)$$

with λ_{wall} thermal conductivity of the gas, 26E-3 (W/mK)
D_i inside diameter of the tube (m)

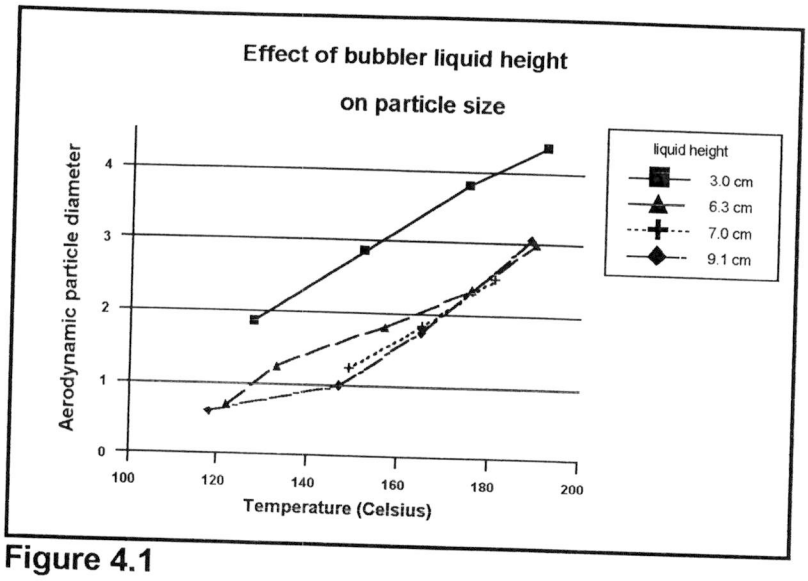

Figure 4.1

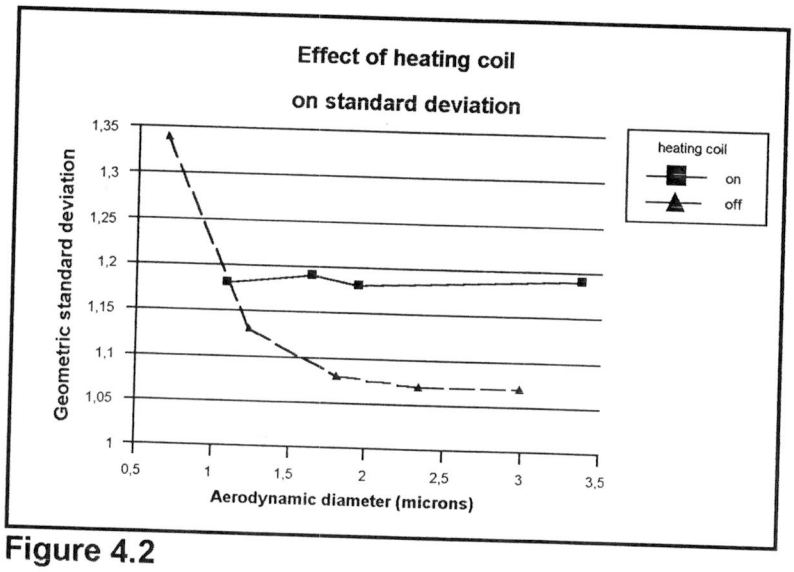

Figure 4.2

4 Experimental Results and Discussion

4.1 Particle Size versus Temperature and Liquid Height

After some preliminary test measurements the aerodynamic particle diameter was measured against temperature for various stearic acid heights in the bubbler. The measurements and conditions are listed in tables 1, 2 and 3 appendix A and the results are shown in figure 4.1. A big difference in particle diameter for a liquid height of 3.0 cm and 6.3 cm can be seen. Assuming that 100% vapour-liquid equilibrium is not reached in the bubbler, a higher liquid level would give a higher equilibrium and so bigger particles. In figure 4.1 the opposite result is shown. For liquids heights over 6.3 cm the particle diameter is more or less the same. For this reason the liquid level in the all following measurements is kept between 6.0 cm and 9.0 cm.

4.2 Monodispersity versus Temperature and the Effect of the Heating Tape

The second objective was to measure the effect of the heating tape on the monodispersity. The heating tape was wrapped around the section after the bubbler till the condenser tube as shown in figure 3.10. The measurements are listed in table 2, appendix A, and presented in figure 4.2. From figure 4.2 it can be seen that condensation without the heating tape produces more monodisperse aerosol. This is in contradiction with theory.

For particles bigger than 1.2 μm, the IMAGE generates particles with a good monodispersity, so in this work the IMAGE is used without heating tape.

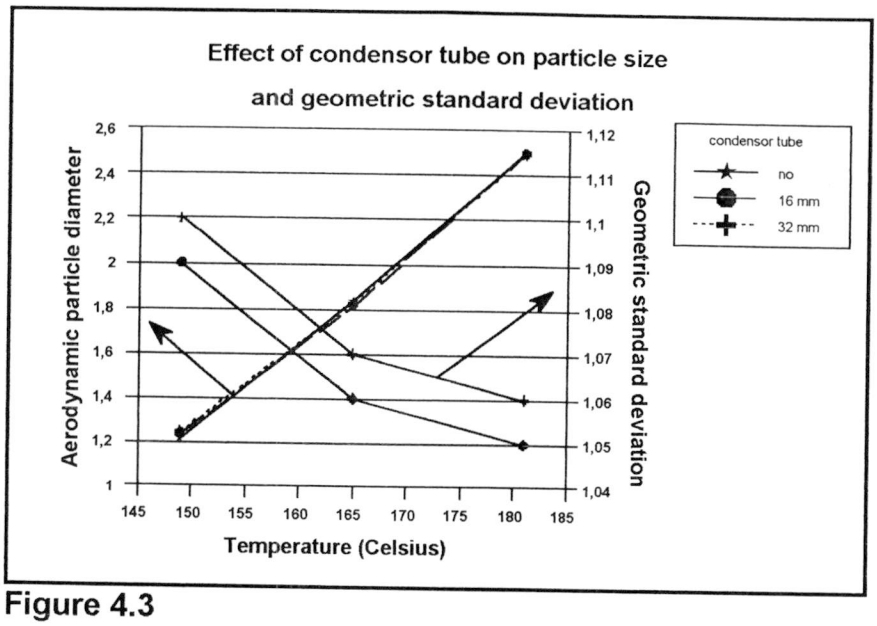

Figure 4.3

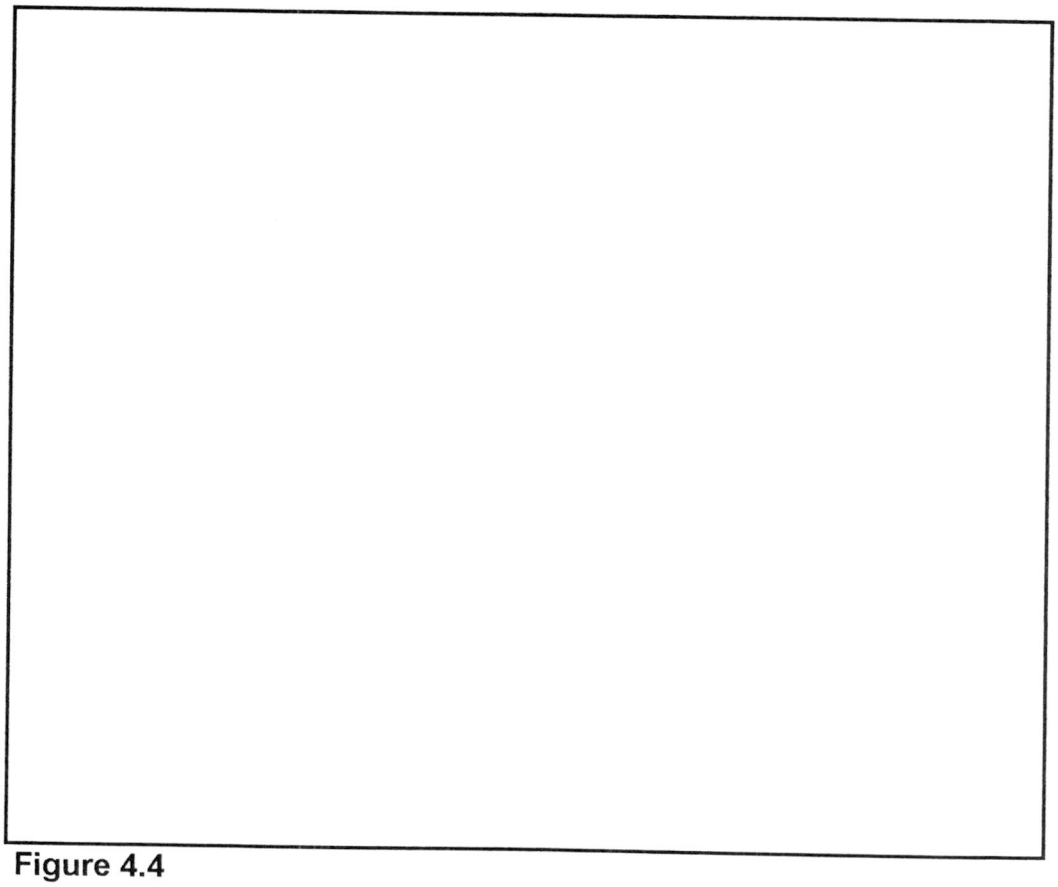

Figure 4.4

4.3 Effect of Condenser Tube on Particle Size and Monodispersity

The effect of the diameter of the condenser on particle size and size distribution was measured at various temperatures. Two condenser tubes were used, one with a internal diameter of 16 mm and one of 32 mm. The results are listed in table 4, appendix A, and presented in figure 4.3. Figure 4.3 shows no significant difference in particle size and monodispersity. This result and the change in monodispersity discussed in paragraph 4.2 indicates that the aerosol is condensed, not in the condenser tube, but in the tube before the condenser tube. For this reason the generated aerosol was measured without the condenser tube. This measurement is also plotted in figure 4.3. No difference can be seen between the aerosol with and without the condenser tubes. This proves that the aerosol is already condensed in the tube before the condenser tube. These condensation conditions can be compared with figure 4.4 for condenser design by Japuntich et al [57]. With an internal diameter of the tube; 7 mm, a gas-flow of 4.8 l/min, and kinematic viscosity of 22.5E-2 cm^2/s at a temperature of 170°C, the Reynolds number is equal to 647. For this temperature the Prandtl number is 0.711 and the Grashoff number is 1.44E4. This condition is not in complete agreement with figure 4.4.

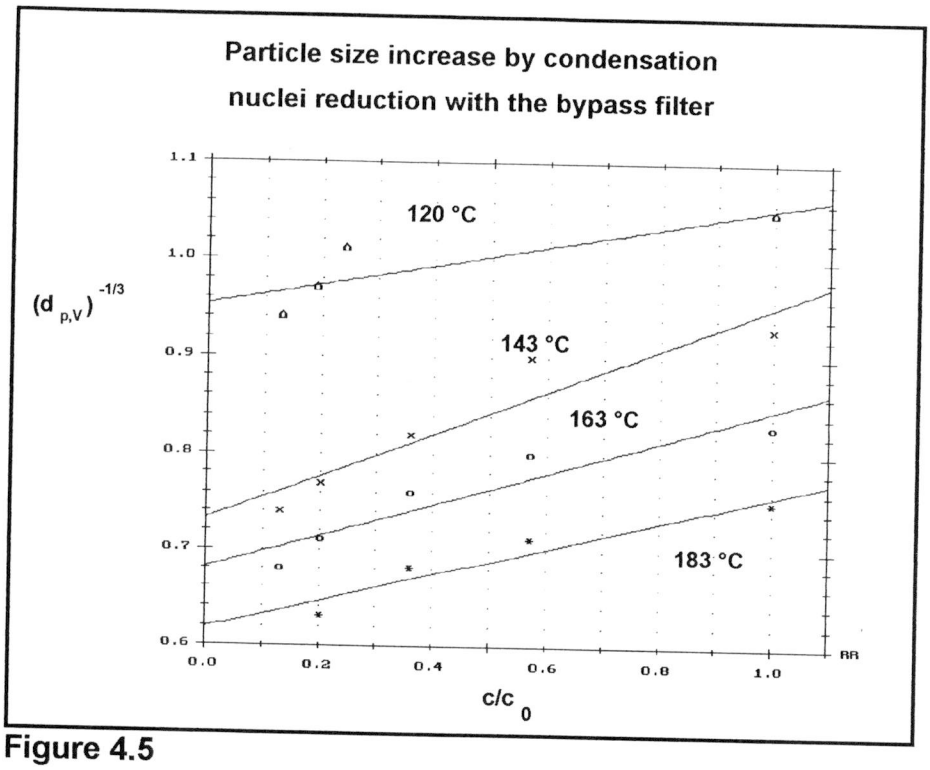

Figure 4.5

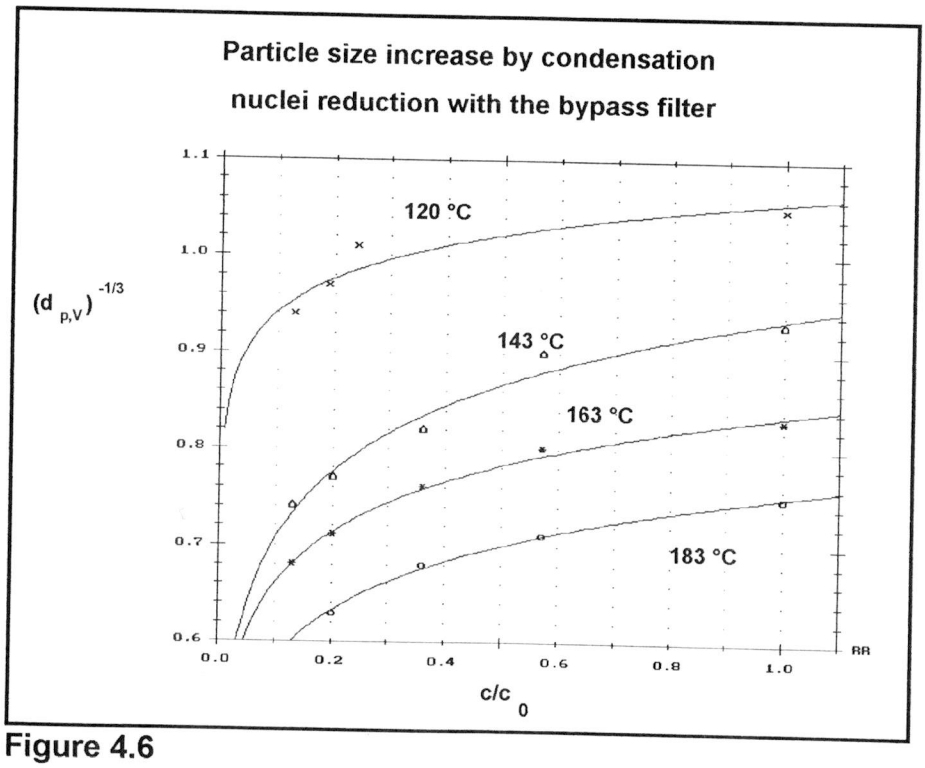

Figure 4.6

4.4 Particle Increase with Condensation Nuclei Filtering

In order to increase the particle diameter, a filter system to decrease in salt-seeds in the nitrogen flow was tested for various temperatures. At a certain temperature, the particle size is given by equation 3.9. According to this equation a plot of $(d_{p,v})^{-1/3}$ versus n/n_0 should give straight lines, where n_0 is the initial salt-seed concentration. The measurements are listed in table 5, appendix A, and presented in figure 4.5. Linear regression lines are fitted to the points. The results of the regression is listed in table 4.1.

Objective:
- coefficients fitted for $(d_{p,v})^{-1/3}=a+b\ n/n_0$

Temperature (°C)	a	b	sum of squares residual ($*10^{-4}$)	correlation coefficient
120	0.953	0.101	17.8	0.86
143	0.732	0.221	28.3	0.95
163	0.681	0.166	17.8	0.94
183	0.618	0.140	6.03	0.96

Table 4.1

Although the fitted lines show a reasonable correlation, the aerosol size is always over-predicted at lower concentration ratios. The data has also been fitted to a logarithmic function. The results of the regression are listed in table 4.2 and presented in figure 4.6.

Objective:
- coefficients fitted for $(d_{p,v})^{-1/3}=a+b\ \log(n/n_0)$

Temperature (°C)	a	b	sum of squares residual ($*10^{-4}$)
120	1.057	0.115	4.41
143	0.936	0.229	2.41
163	0.836	0.175	0.97
183	0.751	0.170	0.25

Table 4.2

From the sum of squares of table 4.1 and 4.2 it can be seen that the logarithmic function gives a better fit.

Bi-modal size distributions were observed for salt-seed concentrations lower than 0.1 n/n_0. The first peek for smaller particles is the result of homogeneous condensation and the second peek for heterogeneous condensation. This occurs sooner literature.

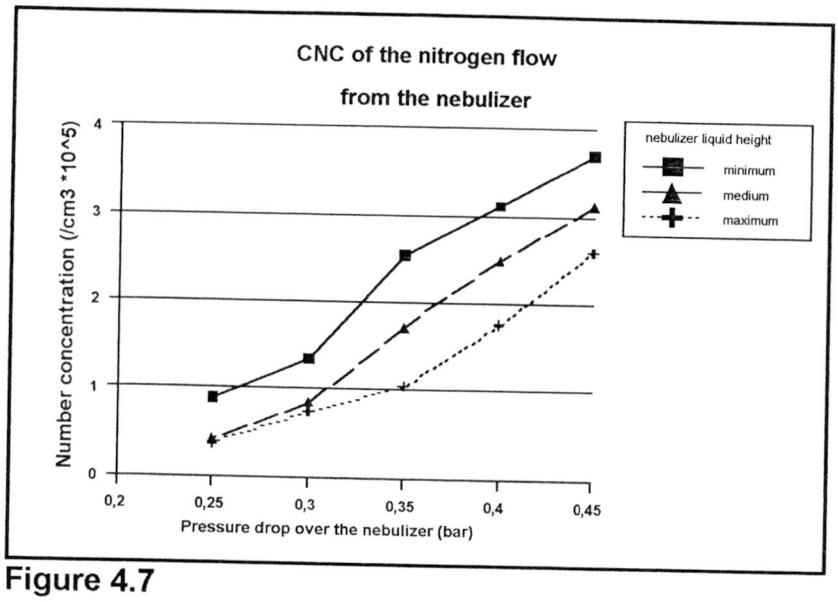

Figure 4.7

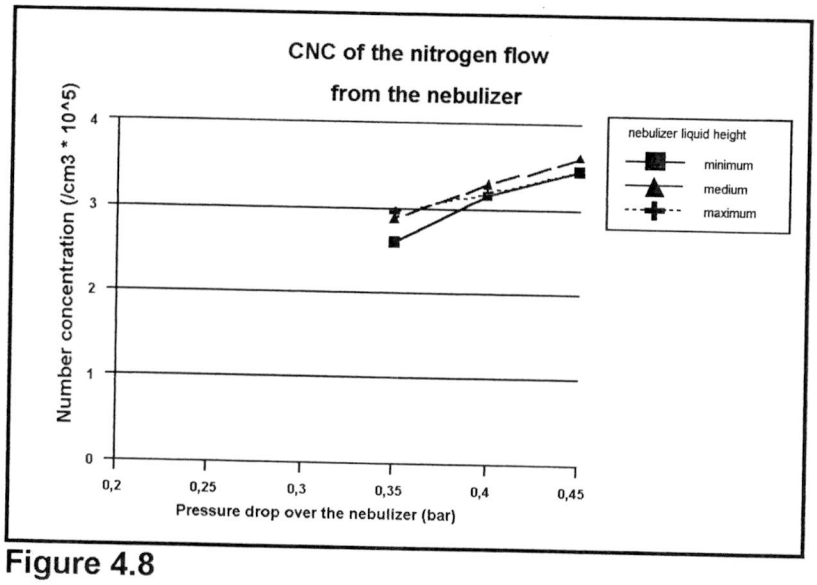

Figure 4.8

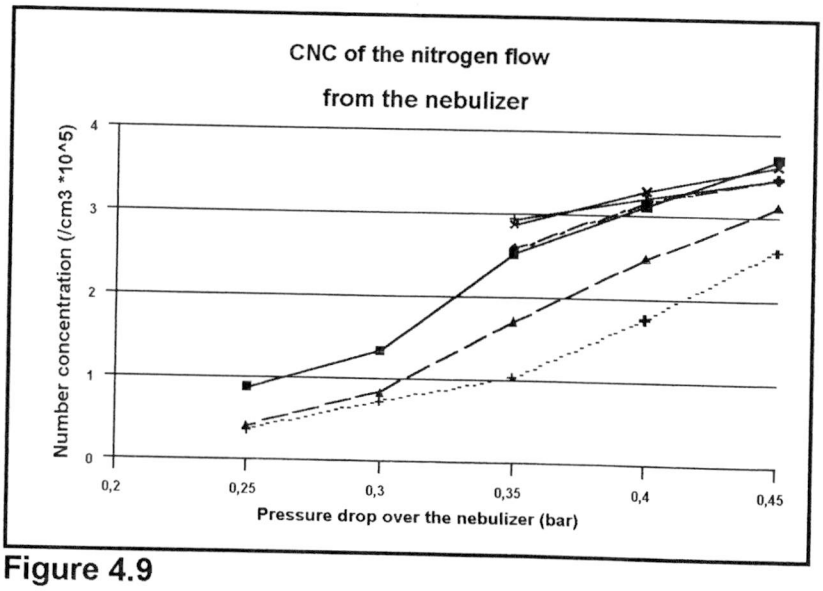

Figure 4.9

4.5 Condensation Nucleation Counting

In order to quantify the number of condensation nuclei generated by the nebulizer, to test the performance of the salt-seed filter and so to implement equation 3.9 a C.N.C. (condensation nucleus counter) was used. The operating principles of the C.N.C. are explained in paragraph 4.2.2. The condensation nuclei were counted for various pressure drops and liquid heights in the nebulizer. The measurements are listed in table 6, appendix A, and presented in figure 4.7. It can be seen that the number concentration increases with decreasing liquid height and pressure drop. Therefore it is very important to keep the liquid around a chosen level.

These measurements were repeated with a new salt-solution. The results of this second test are listed in table 7, appendix A, and presented in figure 4.8. The strong dependence of liquid height on the particle concentration is not found in this measurement. The results of both measurements are shown in figure 4.9.

Measurements of the performance of the salt-seed filter is listed in table 8, appendix A, and presented in figure 4.10. The salt-seed number concentration is measured for different nitrogen flow rates. It can be seen that for smaller flow rates the efficiency is higher. Taking the measurements of table 6, appendix A, as reference, which have an average of $(3.46+3.62+3.46)*10^5/3= 3.51*10^5$ (cm^{-3}) condensation nuclei at 0.45 bar, the efficiency over the total nitrogen flow range is between 97.5-98.2%. In order to reach a higher efficiency a glass fibre filter was used. For a pressure drop over the nebulizer of 0.45 bar and a flow of 4.8 l/min. through the filter a concentration of 39 (cm^{-3}) condensation nuclei was measured downstream of the filter. This represents a filter efficiency of ~100%.

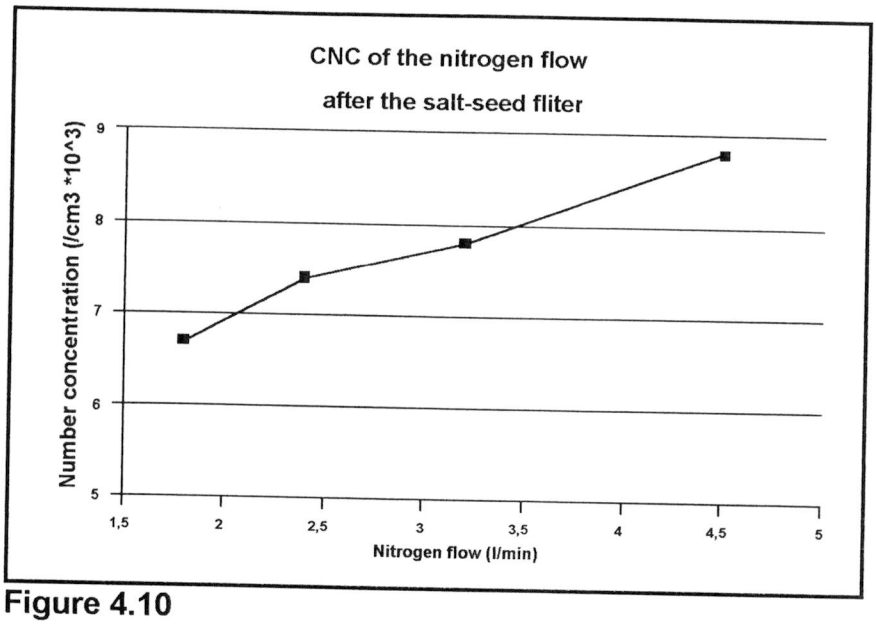

Figure 4.10

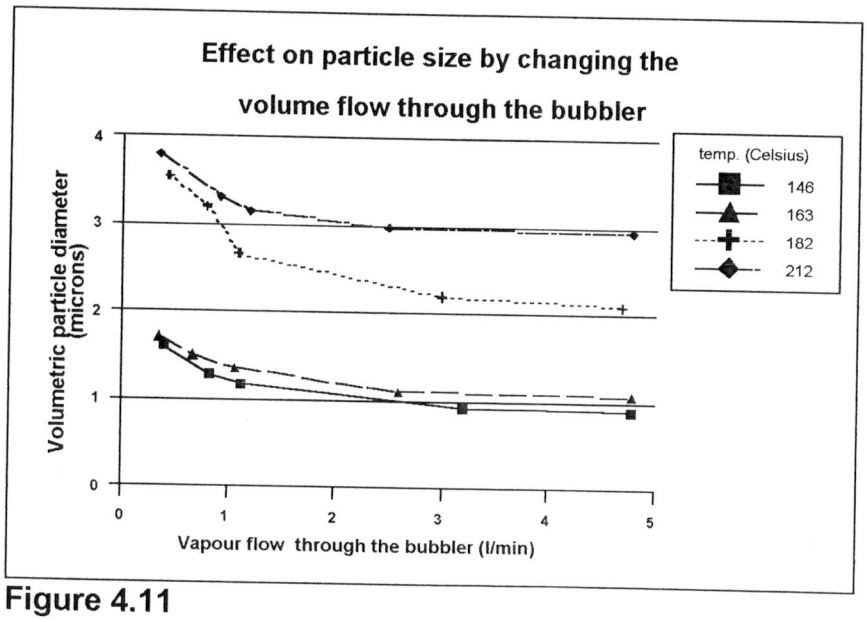

Figure 4.11

4.6 The Effect of Particle Size on Changing the Vapour Flow Through the Bubbler

The effect of liquid height in the bubbler on the particle size as shown in figure 4.1, is probably can be caused by different vapour-liquid equilibrium efficiencies. In order to check whether the equilibrium is 100%, the flow rate through the bubbler is varied. To increase the nitrogen flow through the bubbler, the nitrogen-salt seed flow was split after the diffusion drier, at point 1 in figure 3.1. The results are listed in table 9, appendix A, and presented in figure 4.11. Figure 4.11 show bigger particles at smaller flow rates. This indicates higher vapour-liquid efficiencies at lower flow-rates.

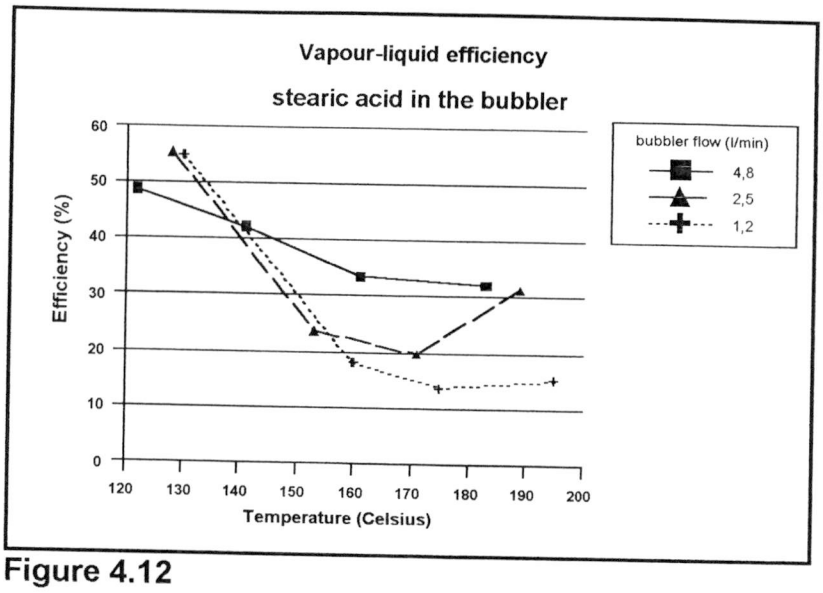

Figure 4.12

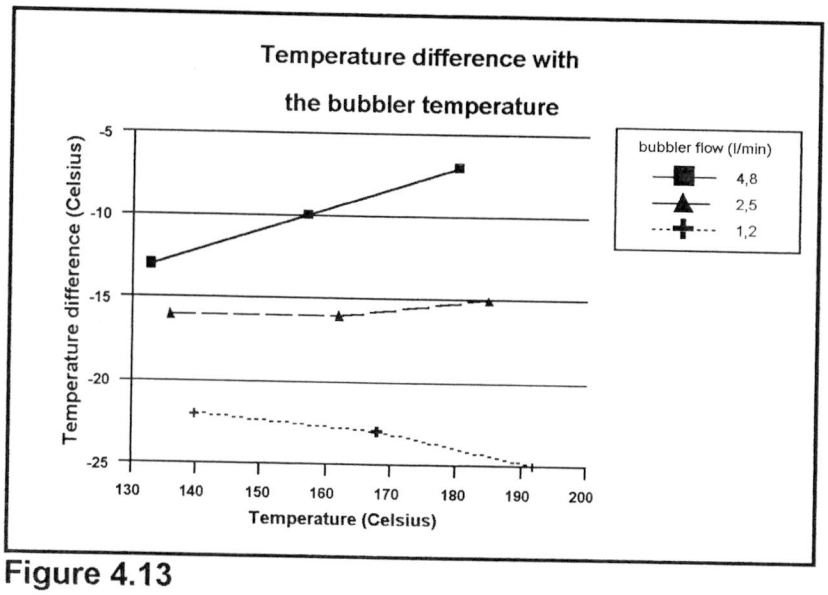

Figure 4.13

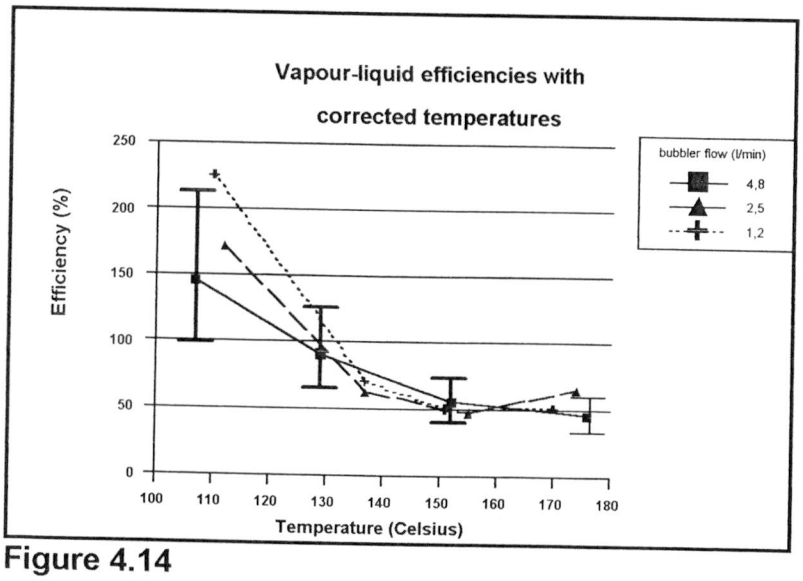

Figure 4.14

4.7 Bubbler Efficiency Measurements

The previous results, bigger particles at lower flow rates, of paragraph 4.6 gave occasion to quantify the bubbler efficiencies for various temperatures and flow-rates. For this reason the generated aerosol was collected on a filter for a fixed time, as described in paragraph 3.6.

The results are listed in table 10, appendix A, and presented in figure 4.12. Figure 4.12 shows higher efficiencies at lower temperatures. The expected higher efficiencies at lower flow-rates are not shown. The opposite result is shown. This strange result is thought to be the result of incorrect temperature measurements. The temperature at the position of the thermometer could not be not the same temperature of the vapour-liquid equilibrium.

A more correct temperature measurement is explained in paragraph 3.3.3. The vapour liquid temperature and the correction found using this improved method of temperature measurement are presented in table 11, appendix A, and the old and corrected temperatures are presented in figure 4.13. The corrected temperature and efficiencies are listed in table 12, appendix A, and presented in figure 4.14. It can be seen that for lower temperatures, the efficiencies rises above the 100%. Although this is incorrect, it can be used to visualise the efficiency-temperature relationship. To visualise the impact of temperature difference on the efficiency, the fault area is plotted for a temperature variance of ± 5 °C for a bubbler flow of 4.8 l/min. Figure 4.12, shows higher efficiencies at lower temperatures. Higher efficiencies at lower flow-rates can not be seen, therefore the particle increase at lower flow rates of figure 4.12, must be the result of increasing temperatures. For example at the temperature of 146 °C the increase in particle mass is $(1.60/0.90)^3$*100%=560%. This can never be caused by a higher vapour-liquid equilibrium at the same temperature alone.

These results show that the preheating section of the bubbler doesn't heat the nitrogen flow to the furnace temperature and the temperature of the nitrogen temperature will change, when the flow rate is changed. This assumption is proved with a computer model of the heat transfer in the preheater. The temperature rise in the preheater is calculated for different flow rates, according to equations 3.5 to 3.8. The results are presented in figure 4.15. Figure 4.15 shows that for flow rates higher than 1.2 l/min the preheater doesn't heat to the furnace temperature.

This difference in temperature could be the cause of the particle diameter change for different liquid heights in the bubbler reported by Horton [1] and shown in figure 4.1. The temperature measured is not the temperature of the vapour liquid equilibrium. Lower liquid levels in the bubbler will result in a higher temperature, which results in bigger particles. For this reason, the performance of the preheater of the MAGE is also calculated according to equations 4.5 to 4.8. The major difference between the MAGE and the IMAGE is the heat transfer coefficient on the outside of the tube. The MAGE concerns forced convection instead of free convection. The heat transfer coefficient on the outside of the tube is equalled to the heat transfer coefficient on the inside of the tube. The length of the tube is 0.75 m and the inner-and outer tube diameter are the same. The results of the calculation are presented in figure 4.16. Due to the lower flow rate in the MAGE, the

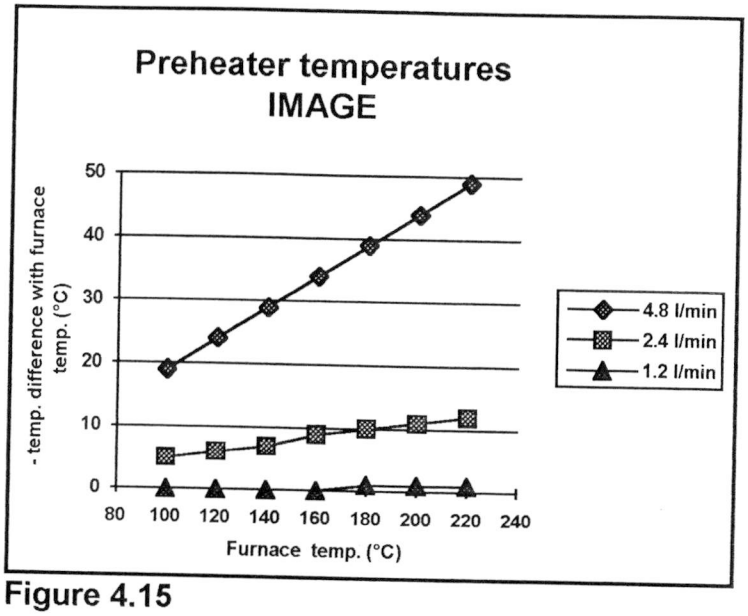

Figure 4.15

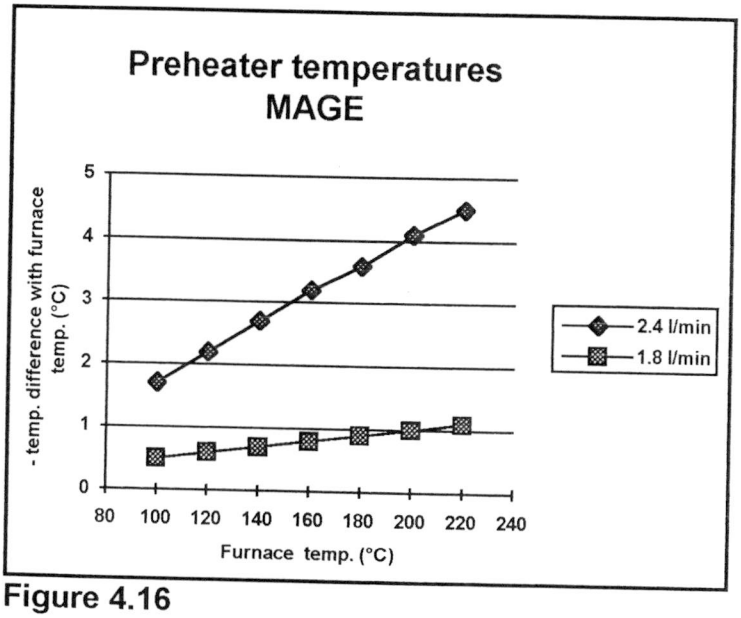

Figure 4.16

temperature difference with the furnace is not as big as with IMAGE but with high temperatures it becomes significantly high. In the mathematical model an ideal situation is described. In reality when the preheater willed be dirty, the difference will be bigger.

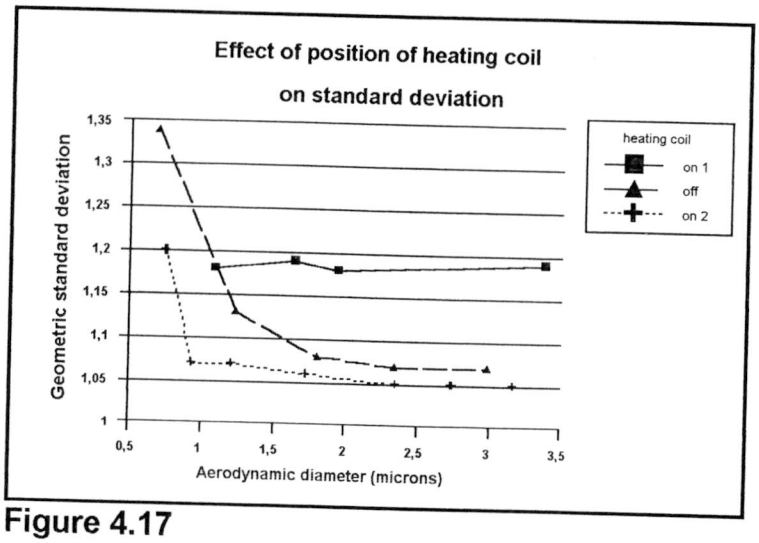
Effect of position of heating coil
on standard deviation
Geometric standard deviation
1,35
1,3
1,25
1,2
1,15
1,1
1,05
1
0,5
1
1,5
2
2,5
3
3,5
Aerodynamic diameter (microns)
heating coil
on 1
off
on 2

Figure 4.17

4.8 Effect of the Position of the Heating Tape on Monodispersity

In order to decrease the aerosol wall losses at the connection between the condenser tube and the bubbler during the efficiency measurements, the heating tape was extended to the first 3 cm of the condenser tube. Measurements of the particle size and geometric standard deviation showed improvement regard to the measurements with the heating tape shown in figure 4.2. The measurement are listed in table 13, appendix A, added to figure 4.2 and presented in figure 4.17. The extension of the heating tape allows better monodispersity than condensation without heating tape. Obviously the narrowing connection before the condenser tube disturbs the laminar flow pattern causing a worsening mondispersity over the hole particle size range.

6 Conclusions

The measurements of the aerosol with and without heating tape showed that the heating tape improves monodispersity, however, it must be wrapped around the section after the bubbler and the first 3 cm of the condenser tube. When the tape is not wrapped around the first part of the condenser tube, the disturbances in laminar flow at the entrance of the condenser tube will worsen the monodispersity

The use of a filter to reduce the condensation nuclei is a very good method to increase the aerosol diameter. Measurements with the condensation nucleus counter showed an 100% efficiency of the filter. The theoretical linear correlation between the particle diameter and the concentration of the condensation nuclei was found. The reduction on the condensation nuclei can, however, done till a reduction of 90%, with the applied nebulizer and pressure drop. This corresponds to a nuclei number concentration of $3.5\ 10^4\ cm^{-1}$.

The change in particle diameter caused by a different liquid height in the bubbler, can only be caused by a different vapour-liquid temperature. In the MAGE and IMAGE the temperature is measured not the bubbler itself, but in the furnace around the bubbler. Measurements of the furnace and bubbler temperature as well as calculations of the temperature rise in the preheater showed a difference in furnace- and bubbler temperature. It is therefore essential to measure and control the temperature in the bubbler instead of the furnace. Changes in the flow rate will then not change the temperature of the vapour liquid equilibrium and the corresponding particle diameter. Even different liquid heights in the bubbler will then not affect particle diameters.

CNC measurements of the nebulizer flow showed dependency of the number concentration on the height of the liquid in the nebulizer. Repeated measurements couldn't confirm the first measurements. It is therefore essential to reinvestigate the stability of the nebulizer, and ultimately the nebulizer should be redesigned to improve stability.

Finally, the IMAGE is a good aerosol generator for particles in a range of 1-4 μm and a monodispersity downto 1.05. Higher temperatures will allow bigger particles. With the suggested changes in temperature measurement and control, the IMAGE is able to produce particles of the same size for at least 1 day.

7 References

1. Horton, R.D. Miller and J.P. Mitchel, Characterisation of a Condensation Type Monodisperse Aerosol Generator (MAGE), Chemistry Division, Winfrith Technology Centre, September 1989, Unclassified.

2. The New Encyclopedia Britannica, Volume 1, 15th edition, 1988, page 121, Encyclopedia Britannica, Inc..

3. Parker C. Reist, Introduction to aerosol science, Macmillan Publishing Company, 1984

4. Fuchs, N.A. and Sutugin, A.G., Chapter 1: "Generation and Use of Monodisperse Aerosols", Aerosol Science (1966), Edited by C.N. Davies, Academic Press, London and N.Y.

5. Worthy, Ward, Aerosol output grew for fifth consecutive year, Chemical & Engineering news (ISSN 0009-2347) v66 p15 May, 16 '88

6. Matijevic, Egon, The world of fine particles, Chemtech (ISSN 0009-2703) v21 p176-81 March '91

7. Pratsinis, Sotris E.; Mastrangelo, Sebastian V. R., Material synthesis in aerosol reactors, Chemical Engineering Progress (ISSN 0360-7275) v85 p62-6, May '89

8. Hinds, W.C.: Aerosol Technology, John Wiley and Sons,Inc., London, (1982), p. 258.

9. Sinclair,D., and LaMer,V.(1949), Chem. Reviews, 44, 245.

10. LaMer,V.(1952),"Air Polution", p.607, New York.

11. LaMer,V.(1952),"Air Polution", p.607, New York

12. LaMer,V.,and Hochberg,S.(1949), Chem.Rev.44, 341, Reviews, 44, 245.

13. Kogan,I. and Burnasheva,S.(1960), Zh.fiz.Khim.34,2630.

14. Pearson,R. and Langer,G.(1960), Nature,Lond.187,235.

15. Goyer,G., and Handler,G. (1955),J.Met.12,596.

16. Hinze,J.,and Milborn,H.(1950),J.Appl.Mech. 17,145.

17. O'Konski,C., and Doyle,C.(1955), Analyt.Chem.27, 694.

18. Stern,S.,Baumstark,J.,Schekman,A.,and Olson,R.(1959),J.Appl.Phys.30,952.

19. Edwards,C.,Evans,L.,and LaMer,V. (1962), J.Colloid Sci. 17,749.

20. Hong, N.S., Jones, A.R., (1976), J.Phys.D. 9, 1839.

21. Chen, B.T., Cheng, Y.S. and Yeh, H.C., (1985), Aerosol Sci. Tech. 4 (1),89.

22. Vanck R., Luck H., Bernigau N. (1990), Advanced techniques of the fredholm integral equation for the determination of the particle size distributions. Proc. 3rd int. Aerosol conference, Pergamon Press, N.Y.

23. Beckord P., Luck H.O., Hoefelmann G., J. Aerosol Sci., Vol.23, Suppl.1, pp. S317-S320, 1992, Pergamon Press Ltd.

24. Sinclair, D. and V.K. LaMer: "Light Scattering as a Measure of Particle Size in Aerosols", Chem. Rev. 44, (1949).

25. Sinclair, D.: "Aerosols, a Personal Remembrance", J. Of Colloid and Interface Science 69, No. 3 (1979), p. 430.

26. Wilson, I.B. and LaMer, V.K.: "The Retention of Aerosol Particles in the Human Respiratory Tract as a Function of Particle Radius", J. Ind. Hyg. Toxicol, 30 (1948), p. 265.

27. Kerker, M.: "Laboratory Generation of Aerosols", Advances in Colloid and Interface Science 5 (2) (1975), p. 105-172.

28. Muir, D.C.F.: "The Production of Monodispersed Aerosols by a LaMer Sinclair Generator", Ann. Occup. Hyg., 8 (196S), pp. 233-8.

29. Wooding, E.R.: "The Physical Properties of Aerosols", Thesis London University (1953).

30. Huang, C.M., Kerker, M., Matijevic, E., and Cooke, D.D., J. Colloid Interface Sci. 33 (1970), p. 244.

31. Smaldone, G.C., Itoh, H., Swift, D.L., Kaplan, J., Florek, R., Wells, W., Wagner, H.N.: "Production of Pharmacologic Monodisperse Aerosols", J. of Applied Physiology - Respiratory Environmental and Exercise Physiology 54 N2, (1983), p. 393-399.

32. Perry, D.G. and Smaldone, G.C.: "Factors Affecting Aerosol Production from a Modified Sinclair-LaMer Aerosol Generator", J. Aerosol Science 16, No. 5, (1985), p. 427

33. Swift, D.L.: Ann. Occup. Hyg. 10, (1967), p. 337.

34. Kogan, Y.I, and Burnasheva, Z.A.: "Growth and Measurement of Condensation Nuclei in a Continuous Stream", Russian J. of Physical Chemistry 34, (1960), p. 2630.

35. Okada, T., Ishibashi, H., Kitani, S.: J. Colloid Interface Science 29, (1969), p. 613.

36. Prodi, V.: "A Condensation Aerosol Generator for Solid Monodisperse Particles", Assessment of Airborne Particles, (1972), edited by T.T. Mercer, P.E. Morrow, W. Stober, C.C. Thomas Publ., Springfield, Illinois, p. 169.

37. Nicolaon, G.D., Cooke, D.D., Kerker, M., Matijevic, E.: "A New Liquid Aerosol Generator", J. Colloid and Interface Science 34 (4), (1970), p. 534.

38. Kerker, M., Matijevic, E., Nicolaon, G., Cooke, D.D.: "Preparation of Liquid Aerosols and their Particle Size Analysis by Light Scattering" Chapter 8, Assessment of Airborne Particles, Ed.: Mercer, T.T., Morrow, P.E., Stober, W., (1972), p. 153, Charles C. Thomas, Sprinqfield, Illinois.

39. Shahriari, S. Sarmiento, A, Goodrich, F.: "The Kinetics of Growth of an Aerosol in a Flow Reactor", J. of Colloid and Interface Science 39, (1972), No. 1, P. 305.

40. Nicolaon, G., Cooke, D.D., Davies, E.J., Kerker, M., Matijevic, E.: J. Colloid Interface Science 35, (1971), p. 490.

41. Nicolaon, G., Kerker, M.: J. Colloid Interface Science 43, (1973), p. 246.

42. Liao, S.C., Ph.D. Thesis: "Condensation Aerosol Formation in Nonuniform Temperature Concentration and Flow Fields", Clarkson College of Technology (1974).

43. Hinds, W., First, M., Gibson, D., Leith, D.: "Size Distribution of Hot DOP Aerosol Produced by ATI-Q-127 Aerosol Generator", p. 1130, Proc. 15th DOE Nuclear Air Cleaning Conference, Conference 780819, (August, 1978).

44. Tu, K.: "A Condensation Aerosol Generator System for Monodisperse Aerosols of Different Physicochemical Properties", J. Aerosol Science 13, No. 5, (1982), pp. 363-371.

45. Gonda, I., Judd, C.D., Cooke, D.D.: "Monodisperse Submicron Glycerine Aerosols", J. of Colloid and Interface Science 68 #2, (1979), p. 396.

46. Sutugin, A.G.: Kolloid Zeitschrift Zh. 27, (1965), p. 545.

47. Rapaport, E., Weinstock, S.G.,: "A Generator for Homogeneous Aerosols", Experimentia Vol. XI/9, 1955, p. 363.

48. Lassen, L.: Z. Angew. Phys. 12, (1960), p. 157.

49. Preining, O.: "Zum Problem der Reichung Fractionierender Messgerate fur Staube der Korngrossen Zwisen 0.1 und 1.0 Micron mit Helfe von Test Aerosolen, Staub 22 (11), (1962), p. 456-63.

50. Berner, A. and Preining, O.: Septieme Colluque sur Possieres L'institut National de Recherche Clinique Appliquee, Paris, (1964), p. 103.

51. Liu, B.Y.H., Whitby, K.T., and Yu, H.H.S.: "A Condensation Aerosol Generator for Producing Monodispersed Aerosols in the Size Range .036 micron to 1.3 micron" Journal de Recherches Atmospheriques 3, (1966), p. 397-406.

52. Tomaides, M., Liu, B.Y.H., Whitby, K.T.: "Evaluation of the Condensation Aerosol Generator for Producing Monodispersed aerosols", Aerosol Science, 2 (1971), pp. 39-46.

53. British Standard 2577, British Standards Institution, 2 Park Street, London, W.I., (1955).

54. Liu, B.Y.H., Lee, K.W.: "Aerosol Generator of High Stability", American Industrial Hygiene Ass'n Journal, 36 N12, (1975), p. 861-865.

55. Little, Inc.: "Design Study of a Filter-testing Dioctyl Phthalate (DOP) Penetrometer", For Sarea-PR-W, U.S. Army Armament Research and Development Command: Aberdeen Proving Ground, Maryland, Contract # DAA 15-76-0-0013, October 31, 1979.

56. Soderholm, S.C., Ortiz, L.W., Nielsen, S.: "Improved Methods of Routinely Measuring Penetration of High Efficiency (HEPA) Filters by Aerosols", Los Alamos National Laboratory Report # LA-10365-PR, May, (1985),p. 77.

57. Japuntich, J.A., Stenhouse, J.I.T. and Liu, B.Y.H., Journal of Colloid and Interface Science, Vol. 136, No.2, May 1990, Conditions for Monodispersity of Hetrogeneous Condensation.

Apendix

Tables

Objectives:

- Measuring the effect of the heating tape on the geometric standard deviation
- Effect of the liquid level in the bubbler on particle size

Liquid level in the bubbler:	3 cm
ΔP over the nebulizer:	0.45 bar
Condensor tube:	16 mm
Flow through the filter	0 l/min
Flow through the bubbler	4.8 l/min

T (°C)	heating tape	d_p (μm)	σ_g
131	on	1.67 1.63 1.67	1.20 1.21 1.20
128	off	1.86 1.86 1.87	1.07 1.07 1.07
150	on	2.60 2.65 2.64	1.20 1.21 1.21
152	off	2.84 2.86 2.86	1.06 1.05 1.05
175	on	3.50 3.26 3.38	1.14 1.19 1.19
175	off	3.80 3.81 3.75	1.05 1.05 1.05
191	on	3.84 3.74 3.85	1.11 1.15 1.13
192	off	4.36 4.33 4.30	1.05 1.05 1.05

Table 1

Objectives:

- Measuring the effect of the heating tape on the geometric standard deviation
- Effect of the liquid level in the bubbler on particle size

Liquid level in the bubbler:	6.3 cm
ΔP over the nebulizer:	0.45 bar
Condensor tube:	16 mm
Flow through the filter	0 l/min
Flow through the bubbler	4.8 l/min

T (°C)	heating tape	d_p (µm)	σ_g
122	off	0.69 0.69 0.70	1.34 1.34 1.37
120	on	1.06 1.09 1.09	1.17 1.18 1.19
133	off	1.28 1.22 1.24	1.14 1.13 1.13
133	on	1.64 1.72 1.57	1.19 1.18 1.17
157	off	1.78 1.81 1.84	1.08 1.08 1.08
157	on	1.81 1.94 1.96	1.18 1.18 1.17
176	off	2.33 2.34 2.36	1.07 1.07 1.07
190	off	2.98 2.99 3.01	1.07 1.07 1.07

Table 2

Objective: • Effect of the liquid level in the bubbler on particle size	
Liquid level in the bubbler: ΔP over the nebulizer: Condensor tube: Flow through the filter Flow through the bubbler Heating tape:	9.1 cm 0.45 bar 16 mm 0 l/min 4.8 l/min off

T (°C)	d_p (μm)	σ_g
118	0.61 0.60 0.60	1.18 1.18 1.19
147	0.99 0.99 0.99	1.11 1.10 1.10
165	1.71 1.73 1.73	1.07 1.07 1.07
189	3.05 3.06 3.07	1.06 1.06 1.06

Table 3

Objective:

- Measuring the effect of the condensor tube on the particle size and geometric standard deviation

Liquid level in the bubbler:	7 cm
ΔP over the nebulizer:	0.45 bar
Heating tape:	off
Flow through the filter	0 l/min
Flow through the bubbler	4.8 l/min

T (°C)	Condensor tube	d_p (μm)	σ_g
149	no	1.22 1.22 1.24	1.11 1.10 1.10
149	16 mm	1.23 1.24 1.25	1.09 1.09 1.08
149	32 mm	1.23 1.25 1.25	1.10 1.10 1.10
165	no	1.83 1.84 1.84	1.07 1.07 1.07
165	16 mm	1.82 1.82 1.84	1.06 1.06 1.06
165	32 mm	1.77 1.85 1.83	1.06 1.07 1.07
181	no	2.49 2.50 2.52	1.06 1.06 1.06
181	16 mm	2.49 2.50 2.51	1.06 1.05 1.05
181	32 mm	2.50 2.49 2.48	1.06 1.06 1.06

Table 4

Objective:

- Measuring the effect on particle size by decreasing the condensation nulei with the bypass
-

Condensation tube	16 mm
Liquid level in the bubbler:	6 cm
ΔP over the nebulizer:	0.45 bar
Heating tape:	on
Flow through the bubbler	4.8 l/min

T (°C)	$\phi_{v,bypass}$ (l/min)	c/c_0	d_p (µm)	σ_g	$d_{p,V}$ (µm)	$(d_{p,V})^{-1/3}$ $(\mu m)^{-1/3}$
120	0	1	0.77	1.19		
			0.75	1.20	0.87	1.05
			0.73	1.20		
	3.7	0.24	0.96	1.10		
			0.95	1.10	0.98	1.01
			0.95	1.10		
	3.9	0.19	1.06	1.11		
			1.04	1.10	1.08	0.97
			1.04	1.10		
	4.2	0.13	1.19	1.10		
			1.17	1.09	1.22	0.94
			1.16	1.09		
	4.5	0.06	bi-nodal			
143	0	1	1.20	1.07		
			1.21	1.07	1.24	0.93
			1.21	1.07		
	2	0.57	1.37	1.07		
			1.37	1.07	1.39	0.90
			1.37	1.07		
	3	0.36	1.79	1.06	1.82	0.82
			1.80	1.06		
			1.76	1.06		
	3.8	0.20	2.17	1.06		
			2.12	1.06		
			2.14	1.06	2.17	0.77
	4.1	0.13	2.44	1.06		
			2.46	1.06	2.50	0.74
			2.49	1.06		
	4.5	0.06	bi-nodal			

163	0	1	1.74	1.06		
			1.73	1.06	1.76	0.83
			1.72	1.06		
	2.0	0.57	1.96	1.05	1.98	0.80
			1.99	1.05		
			1.93	1.05		
	3.0	0.36	2.18	1.05		
			2.23	1.05		
			2.22	1.05	2.24	0.76
	3.8	0.20	2.76	1.05		
			2.70	1.05		
			2.76	1.05	2.79	0.71
	4.1	0.13	3.20	1.06		
			3.07	1.05		
			3.17	1.05	3.20	0.68
	4.3	0.06	bi-nodal			
183	0	1	2.30	1.05		
			2.35	1.05		
			2.34	1.07	2.39	0.75
	2.0	0.57	2.79	1.05		
			2.74	1.05	2.77	0.71
			2.70	1.05		
	3.0	0.36	3.20	1.06	3.25	0.68
			3.22	1.05		
			3.17	1.05		
	3.8	0.20	3.90	1.08		
			4.09	1.09		
			3.92	1.09	4.04	0.63
	4.1	0.13	bi-nodal			

Table 5

Ojective:

- Measuring the number concentration of the condensation nuclei produced in the nebulizer with the CNC

nebulizer liquid height	pressure drop over the nebulizer (bar)	number concentration of condensation nuclei ($-/cm^3$) $\bullet 10^5$
minimum	0.45	3.70
	0.40	3.12
	0.35	2.53
	0.30	1.34
	0.25	0.88
medium	0.45	3.13
	0.40	2.49
	0.35	1.71
	0.30	0.84
	0.25	0.42
maximum	0.45	2.59
	0.40	1.76
	0.35	1.04
	0.30	0.73
	0.25	0.37

Table 6

Ojective: • Measuring the number concentration of the condensation nuclei produced in the nebulizer		
nebulizer liquid height	pressure drop over the nebulizer (bar)	number concentration of condensation nuclei ($-/cm^3$) $\bullet 10^5$
minimum	0.45 0.40 0.35	3.46 3.16 2.60
medium	0.45 0.40 0.35	3.62 3.30 2.88
maximum	0.45 0.40 0.35	3.46 3.20 2.95

Table 7

Ojective: • Measuring the performance of the bypass filter with the CNC	
Pressuredrop over the nebulizer:	0.45 bar
Volum flow through the filter	number concentration of condensation nuclei ($-/cm^3$) $\bullet 10^3$
4.5 3.2 2.4 1.8	8.8 7.8 7.4 6.7

Table 8

Objective:

- Measuring the effect on particle size by changing the volume flow through the bubbler

Liquid level in the bubbler:	6 cm
ΔP over the nebulizer:	0.45 bar
Heating tape:	off
Flow through the filter	0 l/min
Condensor tube	16 mm

T (°C)	ϕ_V (l/min)	d_p (μm)	$d_{p,V}$ (μm)	σ_g
146	0.4	1.58 1.58 1.57	1.60	1.07 1.06 1.06
146	0.83	1.25 1.25 1.24	1.28	1.08 1.08 1.08
146	1.13	1.15 1.14 1.13	1.17	1.08 1.08 1.08
146	3.2	0.92 0.88 0.87	0.93	1.14 1.12 1.11
146	4.8	0.85 0.84 0.84	090	1.13 1.13 1.12
163	0.35	1.71 1.69 1.68	1.71	1.06 1.05 1.05
163	0.67	1.50 1.48 1.47	1.50	1.06 1.06 1.06
163	1.07	1.35 1.34 1.34	1.36	1.06 1.06 1.06
163	2.6	1.07 1.07 1.07	1.10	1.08 1.08 1.08
163	4.8	1.02 1.02 1.04	1.07	1.11 1.11 1.11
182	0.43	3.41 3.47 3.51	3.54	1.08 1.07 1.07
182	0.8	3.15 3.13 3.11	3.2	1.07 1.07 1.07
182	1.1	2.63 2.61 2.59	2.66	1.07 1.07 1.07
182	3.0	2.16 2.16 2.15	2.19	1.08 1.06 1.06
182	4.7	2.03 2.05 2.08	2.09	1.07 1.07 1.07
212	0.35	3.71 3.73 3.70	3.79	1.07 1.06 1.06
212	0.92	3.26 3.30 3.21	3.31	1.06 1.06 1.06
212	1.2	3.09 3.12 3.20	3.15	1.06 1.05 1.07
212	2.5	2.91 2.94 2.93	2.98	1.07 1.07 1.06
212	4.8	2.90 2.87 2.96	2.94	1.06 1.07 1.06

Table 9

Objective: • Aerosol collections for vapour-liquid measurements				
Condensation tube Liquid level in the bubbler: ΔP over the nebulizer: Heating tape:		16 mm 6.0 cm 0.45 on		
Temperature (°C)	P^{sat} (Pa)	Aerosol theoretical (g/min)•10^{-3}	Aerosol collected (g/min) •10^{-3}	Efficiency (%)
Flow through the bubbler 4.8 (l/m)				
122	5.0	2.1	1.0	48.5
141	18.3	7.3	3.1	42.1
161	61.6	23.3	7.8	33.4
183	200.8	72.3	23.3	32.1
Flow through the bubbler 2.5 (l/m)				
128	7.7	1.6	0.89	55.4
153	38.6	8.3	2.14	25.6
171	107.3	22.3	4.43	19.8
189	270.4	54.1	16.6	31.3
Flow through the bubbler 1.2 (l/m)				
130	8.8	0.90	0.49	54.8
160	58.1	5.51	0.99	18.0
175	132.9	12.1	1.66	13.6
195	360.7	31.6	4.80	15.2

Table 10

Objective: • Temperature correction measurements	
Temperature (°C)	Temperature difference (°C)
Flow through the bubbler 4.8 (l/min)	
133 157 180	-13 -10 -7
Flow through the bubbler 2.5 (l/min)	
136 162 185	-16 -16 -15
Flow through the bubbler 1.2 (l/min)	
140 168 192	-22 -23 -25

Table 11

Objective:

- Vapour-liquid calculations with corrected temperatures

Temperature (°C)	P^{sat} (Pa)	Aerosol theoretical (g/min)•10^{-3}	Aerosol collected (g/min) •10^{-3}	Efficiency (%)
Flow through the bubbler 4.8 (l/m)				
107	1.6	0.70	1.0	145
129	8.2	3.36	3.1	91.0
152	36.3	14.0	7.7	55.5
176	140.0	51.2	23.2	45.4
Flow through the bubbler 2.5 (l/m)				
112	2.4	0.52	0.89	172
137	14.1	3.18	2..14	62.4
155	43.4	9.38	4.43	47.2
174	126.0	26.0	17.0	65.1
Flow through the bubbler 1.2 (l/m)				
110	2.0	0.22	0.49	225
137	14.1	1.41	0.99	70.3
151	34.2	3.31	1.66	50.2
170	101.7	9.44	4.80	50.9

Table 12

Objective • Geometric standard deviations at various particle diameters	
d_p (μm)	σ_g
0.77 0.75 0.73	1.19 1.20 1.20
0.94 0.94 0.94	1.07 1.07 1.06
1.20 1.21 1.21	1.07 1.07 1.07
1.74 1.73 1.72	1.06 1.06 1.06
2.30 2.35 2.34	1.05 1.05 1.07
2.79 2.74 2.70	1.05 1.05 1.05
3.20 3.22 3.17	1.06 1.05 1.05

Table 13